$K^*(892)^0$ and $\phi(1020)$ production at midrapidity in pp collisions at $\sqrt{s} = 8$ TeV

S. Acharya *et al.*[*]
(ALICE Collaboration)

(Received 16 November 2019; accepted 21 May 2020; published 17 August 2020)

The production of $K^*(892)^0$ and $\phi(1020)$ in pp collisions at $\sqrt{s} = 8$ TeV was measured by using Run 1 data collected by the ALICE collaboration at the CERN Large Hadron Collider (LHC). The p_{T}-differential yields $d^2N/dyd p_{\mathrm{T}}$ in the range $0 < p_{\mathrm{T}} < 20$ GeV/c for K^{*0} and $0.4 < p_{\mathrm{T}} < 16$ GeV/c for ϕ have been measured at midrapidity, $|y| < 0.5$. Moreover, improved measurements of the $K^{*0}(892)$ and $\phi(1020)$ at $\sqrt{s} = 7$ TeV are presented. The collision energy dependence of p_{T} distributions, p_{T}-integrated yields, and particle ratios in inelastic pp collisions are examined. The results are also compared with different collision systems. The values of the particle ratios are found to be similar to those measured at other LHC energies. In pp collisions a hardening of the particle spectra is observed with increasing energy, but at the same time it is also observed that the relative particle abundances are independent of the collision energy. The p_{T}-differential yields of K^{*0} and ϕ in pp collisions at $\sqrt{s} = 8$ TeV are compared with the expectations of different Monte Carlo event generators.

DOI: 10.1103/PhysRevC.102.024912

I. INTRODUCTION

The study of resonances plays an important role in understanding particle production mechanisms. Particle production at the energies of the CERN Large Hadron Collider (LHC) has both soft- and hard-scattering origins. The hard scatterings are perturbative processes and are responsible for production of high-p_{T} particles, whereas the bulk of the particles are produced due to soft interactions, which are nonperturbative in nature. High-p_{T} particles originate from fragmentation of jets, and their yield can be calculated by folding the perturbative quantum chromodynamics (pQCD) calculations for elementary parton-parton scatterings with universal fragmentation functions determined from experimental data [1–3]. The production yield of low-p_{T} particles cannot be estimated from the first principles of QCD, hence predictions require phenomenological models in the nonperturbative regime. In this paper, we discuss $K^{*0}(892)$ and $\phi(1020)$ production in pp collisions at $\sqrt{s} = 8$ TeV. The $\phi(1020)$ meson is a vector meson consisting of strange quarks ($s\bar{s}$). The production of $s\bar{s}$ pairs was found to be significantly suppressed, compared with $u\bar{u}$ and $d\bar{d}$ pairs in pp collisions due to the larger mass of the strange quark [4,5]. The $K^{*0}(892)$ is a vector meson with a similar mass to the $\phi(1020)$, but differs in strangeness content by one unit, which may help in understanding the strangeness production dynamics. Measurements of particle production in inelastic pp collisions provide input to tune the QCD-inspired Monte Carlo (MC) event generators such as EPOS [6], PYTHIA [7] and PHOJET [8,9]. Furthermore, the measurements in inelastic pp collisions at $\sqrt{s} = 8$ TeV reported in this paper serve as reference data to study nuclear effects in proton-lead (p-Pb) and lead-lead (Pb-Pb) collisions.

In this article, the p_{T}-differential and p_{T}-integrated yields and the mean transverse momenta of $K^{*0}(892)$ and $\phi(1020)$ at midrapidity in pp collisions at $\sqrt{s} = 8$ TeV are presented. The energy dependence of the p_{T} distributions and particle ratios to the yields of charged pions and kaons in pp collisions is examined and discussed. The yields of pions and kaons measured previously by ALICE [10–12] at $\sqrt{s} = 0.9$, 2.76, and 7 TeV are used to obtain the yields in pp collisions at $\sqrt{s} = 8$ TeV. Moreover, updated measurements of the $K^{*0}(892)$ and $\phi(1020)$ at $\sqrt{s} = 7$ TeV are presented; our first measurements for that collision system were published in Ref. [13]. These results include an extension of the $K^{*0}(892)$ measurement to high p_{T} and an improved re-analysis of $\phi(1020)$. This measurement has updated track-selection cuts, which are identical to those described for the measurements at $\sqrt{s} = 8$ TeV, has an improved estimate of the systematic uncertainties, and extends to greater values of p_{T}. Throughout this paper, the results for $K^*(892)^0$ and $\overline{\mathrm{K}}^*(892)^0$ are averaged and denoted by the symbol K^{*0}, while $\phi(1020)$ is denoted by ϕ unless specified otherwise.

This article is organized as follows: The experimental setup is briefly explained in Sec. II and the analysis procedure is given in Sec. III. The results and discussions are presented in Sec. IV followed by the conclusions in Sec. V.

II. EXPERIMENTAL SETUP

The ALICE detector can be used to reconstruct and identify particles over a wide momentum range, thanks to the low material budget, the moderate magnetic field (0.5 T) and the presence of detectors with excellent particle identification (PID) techniques. A comprehensive description of the detector

[*]Full author list given at the end of the article.

and its performance during Run 1 of the LHC is reported in Refs. [14,15].

The detectors used for this analysis are described in the following. The V0 detectors are two plastic scintillator arrays used for triggering and event characterization. They are placed along the beam direction at 3.3 m (V0A) and −0.9 m (V0C) on either side of the interaction point with a pseudorapidity coverage of $2.8 < \eta < 5.1$ and $-3.7 < \eta < -1.7$, respectively. The inner tracking system (ITS), which is located between 3.9 and 43 cm radial distance from the beam axis, is made up of six layers of cylindrical silicon detectors (two layers of silicon pixels, two layers of silicon drift, and two layers of double-side silicon strips). Because it provides high-resolution space points close to the interaction point, the momentum and angular resolution of the tracks reconstructed in the time projection chamber (TPC) is improved. The TPC is the main tracking device covering full azimuthal acceptance and the pseudorapidity range $-0.9 < \eta < 0.9$. It is a 92 m^3 cylindrical drift chamber filled with an active gas. It is divided into two parts by a central cathode, and the end plates consist of multiwire proportional chambers. The TPC is also used for particle identification via the measurement of the specific ionization energy loss (dE/dx) in the gas. The time-of-flight (TOF) detector surrounds the TPC and consists of large multigap resistive plate chambers. It has pseudorapidity coverage $-0.9 < \eta < 0.9$, full azimuthal acceptance, and an intrinsic time resolution of < 50 ps. The TOF is used for particle identification at intermediate momenta. The particle identification techniques based on the TPC and TOF signals are presented in detail in the next section.

III. DATA ANALYSIS

The measurements of K^{*0} and ϕ meson production in pp collisions at $\sqrt{s} = 8$ TeV (7 TeV) were performed during Run 1 data taking with the ALICE detector in 2012 (2010) using a minimum bias trigger, as discussed in Sec. III A. A total of around 45 M events were analyzed for both $\sqrt{s} = 7$ and 8 TeV and the corresponding integrated luminosities are 0.72 and 0.81 nb^{-1}, respectively. The K^{*0} and ϕ resonances are reconstructed via their hadronic decay channels with large branching ratios (B): $K^{*0} \to \pi^{\pm}K^{\mp}$ with $B = 66.6\%$ and $\phi \to K^{+}K^{-}$ with $B = 49.2\%$ [16]. Some older measurements of ϕ used a value of 48.9% for the $\phi \to K^{+}K^{-}$ branching ratio [17]; when comparing different ϕ measurements, the older results are scaled to account for the new branching ratio.

A. Event and track selection

For pp collisions at $\sqrt{s} = 8$ TeV, the events were selected with a minimum bias trigger based on a coincidence signal in V0A and V0C. For pp collisions at $\sqrt{s} = 7$ TeV, the trigger condition is same as in Ref. [13]. The ITS and TPC are used for tracking and reconstruction of charged particles and of the primary vertex. Events having the primary vertex coordinate along the beam axis within 10 cm from the nominal interaction point are selected. Pile-up events are rejected if more than one vertex is found with the silicon pixel detector (SPD). A primary track traversing the TPC induces signals on a maximum of 159 tangential pad-rows, each corresponding to one cluster used in track reconstruction. For this analysis, high-quality charged tracks are used to select pion and kaon candidates coming from the decays of K^{*0} and ϕ. Tracks are required to have at least 70 TPC clusters and a χ^2 per track point ($\chi^2/N_{\text{clusters}}$) of the track fit in the TPC less than four. Moreover, tracks must be associated with at least one cluster in the SPD. To ensure a uniform acceptance by avoiding the edges of the TPC, tracks are selected within $|\eta| < 0.8$. To reduce contamination from secondary particles coming from weak decays, cuts on the distance of closest approach to the primary vertex in the transverse plane (DCA_{xy}) and longitudinal direction (DCA_z) are applied. The value of DCA_{xy} is required to be less than seven times its resolution: $\text{DCA}_{xy}(p_{\text{T}}) < (0.0105 + 0.035 p_{\text{T}}^{-1.1})$ cm (p_{T} in GeV/c), and DCA_z is required to be less than 2 cm. To improve the global resolution, the p_{T} of each track is chosen to be greater than 0.15 GeV/c.

In the TPC, particles are identified by measuring the dE/dx in the TPC gas, whereas in the TOF it is done by measuring the time of flight. The particles in the TPC are selected by using a cut on the difference of the mean value of the dE/dx to the expected dE/dx value for a given species divided by the resolution σ_{TPC}. This cut is expressed in units of the estimated σ_{TPC}. As described below, this is optimized for each analysis and depends on the signal-to-background ratio and on the transverse momentum. Particles are identified in the TOF by comparing the measured time of flight to the expected one for a given particle species. The cut is expressed in units of the estimated resolution σ_{TOF}. The TOF allows pions and kaons to be unambiguously identified up to momentum $p \approx 1.5$ GeV/c and also removes contamination from electrons. The two mesons can be distinguished from (anti)protons up to $p \approx 2.5$ GeV/c.

For K^{*0} and ϕ reconstruction, three TPC PID selection criteria are used, depending on the momentum of the daughter particle. For pp collisions at $\sqrt{s} = 8$ TeV, both pions and kaons are selected by using a cut of $|N\sigma_{\text{TPC}}| < 2.0$ for $p(K^{\pm}, \pi^{\pm}) > 0.4$ GeV/c. Here, $p(K^{\pm}, \pi^{\pm})$ denotes the momenta of pions and kaons. Similarly, for $p(K^{\pm}, \pi^{\pm}) < 0.3$ GeV/c, a cut of $|N\sigma_{\text{TPC}}| < 6.0$ is applied, while a cut of $|N\sigma_{\text{TPC}}| < 4.0$ for $0.3 < p(K^{\pm}, \pi^{\pm}) < 0.4$ GeV/c is applied. For the new analysis of the K^{*0} (ϕ) at $\sqrt{s} = 7$ TeV, the specific energy loss for pion and kaon candidates is required to be within $2\sigma_{\text{TPC}}$ ($3\sigma_{\text{TPC}}$) of the expected mean, irrespective of the momentum. Also, a TOF $3\sigma_{\text{TOF}}$ veto cut is applied for K^{*0} for both $\sqrt{s} = 7$ and 8 TeV. "TOF veto" means that the TOF 3σ cut is applied only for cases where the track matches a hit in the TOF.

B. Raw yield extraction

The K^{*0} (ϕ) meson is reconstructed through its dominant hadronic decay channel $K^{*0} \to \pi^{\pm}K^{\mp}(\phi \to K^{+}K^{-})$ by calculating the invariant mass of its daughters at the primary vertex. The invariant-mass distribution of the decay daughter pairs is constructed by taking unlike-sign pairs of K and π (K) candidates for K^{*0} (ϕ) in the same event. The rapidity of the πK (KK) pairs is required to lie within the range $|y_{\text{pair}}| < 0.5$. As an example, the πK (KK) invariant-mass distribution for

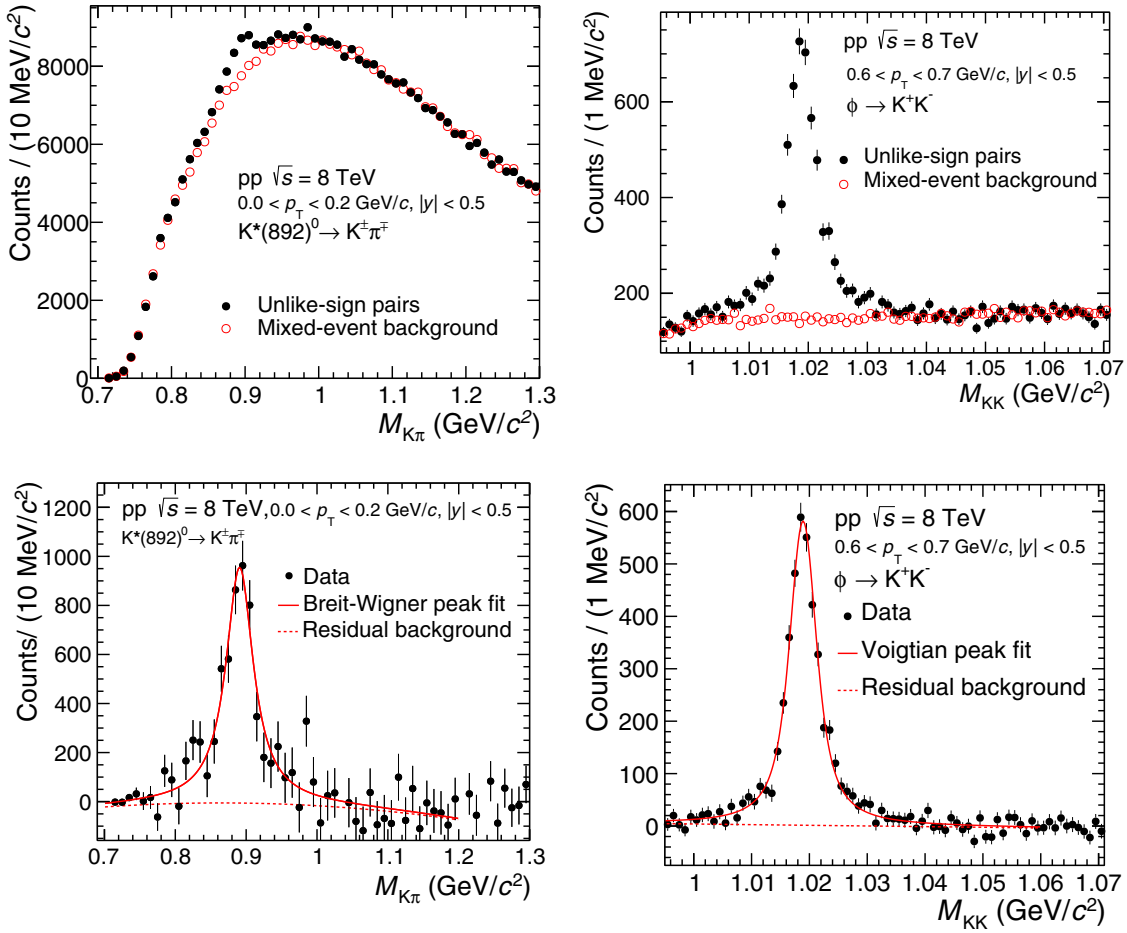

FIG. 1. (Upper panels) Invariant-mass distributions (closed black point) for the K^{*0} (left) and ϕ (right) in pp collisions at 8 TeV in the p_T range $0 < p_T < 0.2$ GeV/c and $0.6 < p_T < 0.7$ GeV/c, respectively. The combinatorial background (open red circles) is estimated by using unlike-sign pairs from different events (mixed events). The statistical uncertainties are shown as bars. (lower panels) $K\pi$ (left) and KK (right) invariant-mass distributions in the same p_T ranges after combinatorial background subtraction together with the fits to the signal and background contribution.

$\sqrt{s} = 8$ TeV is shown in Fig. 1 for $0 < p_T < 0.2$ GeV/c ($0.6 < p_T < 0.7$ GeV/c).

The shape of the uncorrelated background is obtained via the event mixing technique, calculating the invariant-mass distribution of unlike-sign $\pi^\pm K^\mp$ (K^{*0}) or K^+K^- (ϕ) combinations from different events, as shown in the upper panel of Fig. 1. To reduce statistical uncertainties each event was mixed with five other similar events. For $\sqrt{s} = 8$ TeV, the mixed-event background is normalized in the mass range $1.1 < M_{K\pi} < 1.5\,\text{GeV}/c^2$ ($1.04 < M_{KK} < 1.06\,\text{GeV}/c^2$) for $K^{*0}(\phi)$ so that it has the same integral as the unlike-charge distribution in that normalization region. For $\sqrt{s} =$ 7 TeV, the mixed event background is normalized in the mass range $1.1 < M_{K\pi} < 1.15\,\text{GeV}/c^2$ and $1.048 < M_{KK} <$ 1.052 GeV/c^2 for K^{*0} and ϕ, respectively. To avoid mismatches due to different acceptances and to assure a similar event structure, only tracks from events with similar vertex positions ($\Delta z < 1$ cm) and track multiplicities ($\Delta n < 5$) are mixed. For the ϕ meson in pp collisions at $\sqrt{s} = 7$ TeV, the multiplicity difference for event mixing is restricted to $\Delta n \leqslant 10$. This combinatorial background is subtracted from the unlike-charge mass distribution in each p_T bin. Due to an imperfect description of the combinatorial background, as well to the presence of a correlated background, a residual background still remains. The correlated background can arise from correlated $K\pi$ (KK) pairs for $K^{*0}(\phi)$, misidentified particle decays, or jets.

The K^{*0} raw yield is extracted from the $K\pi$ invariant-mass distribution in different p_T bins between 0 and 20 GeV/c. After the combinatorial background subtraction the invariant-mass distribution is fit with the combination of a Breit-Wigner function for the signal peak and a second-order polynomial for the residual background. The fit function for K^{*0} is given by

$$\frac{dN}{dM_{K^\pm\pi^\mp}} = \frac{A}{2\pi}\frac{\Gamma_0}{(M_{K^\pm\pi^\mp} - m_0)^2 + \frac{\Gamma_0^2}{4}} + \left(BM^2_{K^\pm\pi^\mp} + CM_{K^\pm\pi^\mp} + D\right). \quad (1)$$

Here m_0 is the fitted mass pole of the K^{*0}, Γ_0 is the resonance width, and A is the yield of the K^{*0} meson. B, C, and D are the fit parameters in the second-order polynomial.

The ϕ raw yield is extracted from the KK invariant-mass distribution in different p_{T} bins between 0.4 and 16 GeV/c after the combinatorial background subtraction. For the ϕ fit function, the detector mass resolution is taken into account due to the smaller width of the ϕ meson. This is achieved by using a Breit-Wigner function convoluted with a Gaussian function, which is known as Voigtian function. The KK invariant-mass distribution is fit with the combination of a Voigtian function for the signal peak and a second-order polynomial for the residual background. The fit function for ϕ is given by

$$\frac{dN}{dM_{KK}} = \frac{A\Gamma_0}{(2\pi^{3/2})\sigma}\int_{-\infty}^{+\infty}\exp\left(\frac{(M_{KK}-m')^2}{2\sigma^2}\right) \times \frac{1}{(m'-m_0)^2+\frac{\Gamma_0^2}{4}}dm' + \left(BM_{KK}^2 + CM_{KK} + D\right). \tag{2}$$

Here m_0 is the fitted mass pole of ϕ, Γ_0 is the resonance width fixed to the value in vacuum, and σ is the p_{T}-dependent mass resolution, which ranges from 1 to 3 MeV/c^2.

To extract the raw yields of K^{*0} (ϕ), for each p_{T} bin the invariant-mass histogram is integrated over the region $0.801 < m_{K^{*0}} < 0.990$ ($1.01 < m_{\phi} < 1.03$), i.e., a range of two to three times the nominal width around the nominal mass. The integral of the residual background function in the same range is then subtracted. The resonance yields beyond the histogram integration regions are found by integrating the tails of the signal fit function; these yields are then added to the peak yield computed by integrating the histogram.

C. Normalization and correction

The K^{*0} and ϕ raw yields N_{raw} are normalized to the number of inelastic pp collisions and corrected for the branching ratio (B), vertex selection, detector geometric acceptance A, efficiency ε, and signal loss. The K^{*0} and ϕ corrected yields are obtained by

$$\frac{d^2N}{dp_{\mathrm{T}}dy} = \frac{N_{\mathrm{raw}}\,\epsilon_{\mathrm{SL}}}{N_{\mathrm{evt}}\,B dp_{\mathrm{T}}dy\,\varepsilon_{\mathrm{rec}}} f_{\mathrm{norm}} f_{\mathrm{vtx}}. \tag{3}$$

Here $\varepsilon_{\mathrm{rec}} = A\varepsilon$ is the correction that accounts for the detector acceptance and efficiency. ϵ_{SL} is the signal loss correction factor and accounts for the loss of $K^{*0}(\phi)$ mesons incurred by selecting events that satisfy only the ALICE minimum bias trigger, rather than all inelastic events. This is a particle species and p_{T}-dependent correction factor which is peaked at low p_{T}, indicating that events that fail the trigger selection have softer p_{T} spectra than the average inelastic event. The signal loss correction factor is about 1% at low p_{T} and negligible for $p_{\mathrm{T}} > 1$ GeV/c. This correction is the ratio of the p_{T} spectrum from inelastic events to the p_{T} spectrum from triggered events and it is evaluated by using Monte Carlo simulations.

N_{evt} is the number of triggered events and a trigger efficiency f_{norm} is used to normalize the yield to the number of inelastic pp collisions. The value of the inelastic normalization factor for pp collisions at $\sqrt{s} = 8$ TeV is 0.77 ± 0.02, which is the ratio between the V0 visible cross section [18] and the inelastic cross section [19]. Similarly, we correct the yield with f_{vtx}, which is the ratio of the number of events for which a good vertex was found to the total number of triggered events. This is estimated to be 0.972. The new results at 7 TeV are normalized as in Ref. [13].

The $\varepsilon_{\mathrm{rec}}$ correction factor is determined from a Monte Carlo simulation using PYTHIA8 as the event generator and GEANT3 [20] as the transport code for the simulation of the detector response. $\varepsilon_{\mathrm{rec}}$ is obtained as the fraction of K^{*0} and ϕ reconstructed after passing the same event selection and track quality cuts as used for the real events to the total number of generated resonances. This $\varepsilon_{\mathrm{rec}}$ value is small at low p_{T} and increases with increasing p_{T}. This value is independent of p_{T} above 5–6 GeV/c [13].

TABLE I. Systematic uncertainties in the measurement of K^{*0} and ϕ yields in pp collisions at $\sqrt{s} = 7$ and 8 TeV. The global tracking uncertainty is p_{T} independent, while the other single-valued systematic uncertainties are averaged over p_{T}. The values given in ranges are minimum and maximum uncertainties depending on p_{T}.

	pp, $\sqrt{s} = 8$ TeV		pp, $\sqrt{s} = 7$ TeV	
Source	K^{*0} (%)	ϕ (%)	K^{*0} (%)	ϕ (%)
Signal extraction	8.7	1.9	8.5	4.0
Track selection	4.0	2.0	5.8	3.2
Material budget	0–3.4	0–5.4	0–3.4	0–5.4
Hadronic interaction	0–2.8	0–3.1	0–2.8	0–3.1
Global tracking efficiency	6.0	6.0	8.0	8.0
Branching ratio	Neg.	1.0	Neg.	1.0
Total	11.3–12.1	6.7–9.1	9.2–18.3	9.1–15.4

D. Systematic uncertainties

The systematic uncertainties on the p_{T}-differential yield, summarized in Table I, are due to different sources such as signal extraction, background subtraction, track selection, global tracking uncertainty, knowledge of the material budget, and the hadronic interaction cross section.

The systematic uncertainties associated with the signal extraction are estimated by varying the fitting ranges, the order of residual backgrounds (from first order to third order), the width parameter and the mixed-event background-normalization range. The signal extraction systematic uncertainties also include the background subtraction systematic uncertainties, which are estimated by changing the methods used to estimate the combinatorial background (like sign and event mixing). The PID cuts and the track quality selection criteria are varied to obtain the systematic uncertainties due to the track selection. The relative uncertainties due to signal extraction and track selection for K^{*0} (ϕ) are 8.7% (1.9%) and 4% (2%), respectively, at $\sqrt{s} = 8$ TeV.

The global tracking uncertainty is calculated by using ITS and TPC clusters for charged decay daughters. The relative systematic uncertainty due to the global tracking efficiency is 3% for charged particles, which results in a 6% effect for the πK and KK pairs used in the reconstruction of the K^{*0} and ϕ,

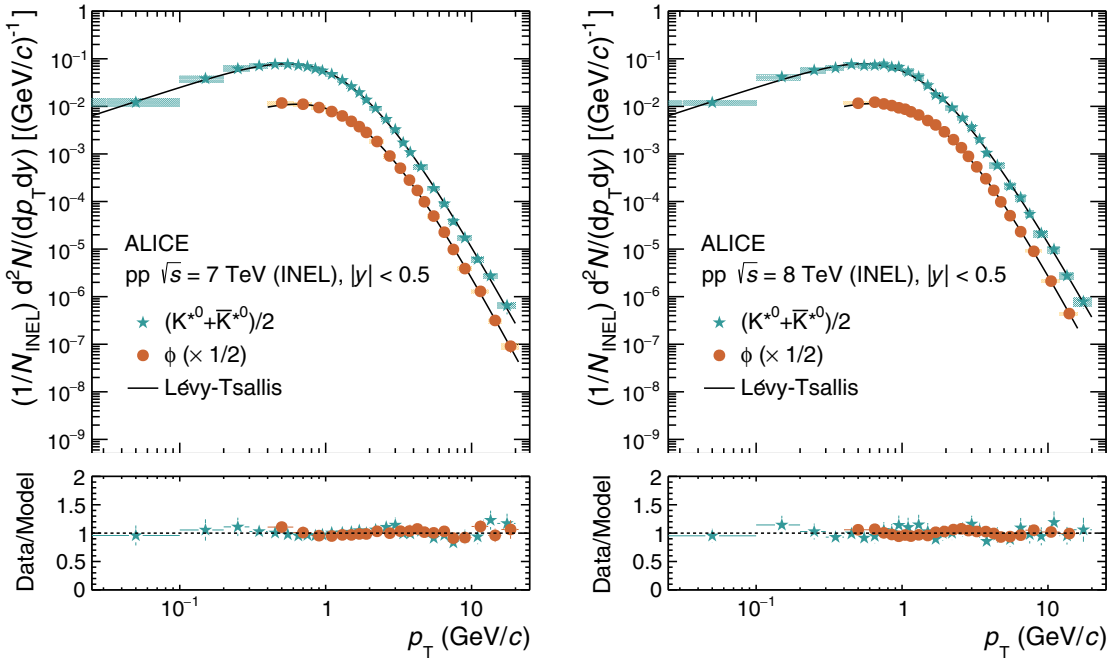

FIG. 2. Upper panels shows the p_T spectra of K^{*0} and ϕ in inelastic pp collisions at 7 TeV (left) and 8 TeV (right) and fit with the Lévy-Tsallis distribution [23,24]. The normalization uncertainty in the spectra is $^{+7.3}_{-3.5}$% for 7 TeV and 2.69% for 8 TeV. The vertical bars show statistical uncertainties and the boxes show systematic uncertainties. The lower panels show the ratio of data to the Lévy-Tsallis fit. Here, the bars show the systematic uncertainty.

respectively. The systematic uncertainty due to the residual uncertainty in the description of the material in the Monte Carlo simulation contributes up to 3.4% for K^{*0} (5.4% for ϕ). The systematic uncertainty due to the hadronic interaction cross section in the detector material is estimated to be up to 2.8% for K^{*0} and up to 3.1% for ϕ. The uncertainties are accordingly propagated to the K^{*0} and ϕ [21,22]. The total systematic uncertainties, which are found to be p_T dependent, range in from 11.3% to 12.1% for K^{*0} and from 6.7% to 9.1% for ϕ. The uncertainties at $\sqrt{s} = 7$ TeV are similarly estimated, totalling to comparable values, as seen in Table I.

IV. RESULTS AND DISCUSSION

A. Transverse momentum spectra and differential yield ratios

Here, we report the measurement of K^{*0} and ϕ in inelastic pp collisions at $\sqrt{s} = 8$ TeV in the range up to $p_T = 20$ GeV/c for K^{*0} and up to $p_T = 16$ GeV/c for ϕ. Also, we present the new measurements of K^{*0} and ϕ in inelastic pp collisions at $\sqrt{s} = 7$ TeV in the range up to $p_T = 20$ GeV/c for K^{*0} and up to $p_T = 21$ GeV/c for ϕ. The re-analyzed K^{*0} and ϕ spectra in pp collisions at $\sqrt{s} = 7$ TeV agree with the previously published values [13] within a few percent at low p_T. At higher p_T ($\gtrsim 3$ GeV/c for K^{*0} and $\gtrsim 2$ GeV/c for ϕ), the old and re-analyzed results can differ by up to 20%, although their systematic uncertainties still overlap. For both energies, the first bin of K^{*0} starts at $p_T = 0$ GeV/c and for ϕ, it starts at $p_T = 0.4$ GeV/c. In Fig. 2, we show the transverse momentum spectra of K^{*0} and ϕ at midrapidity $|y| < 0.5$ and fit with the Lévy-Tsallis distribution [23,24]. The ratio of the measured data to the Lévy-Tsallis fit shows good agreement of data with model within systematic uncertainties. The fit parameters are shown in Table II.

The energy evolution of the transverse momentum spectra for K^{*0} and ϕ is studied by calculating the ratio of p_T-differential yields for inelastic events at $\sqrt{s} = 7$ and 8 TeV to those at $\sqrt{s} = 2.76$ TeV [25]. This is shown in Fig. 3. The differential yield ratio to 2.76 TeV is consistent for 7 and 8 TeV within systematic uncertainties. The systematic uncertainties at both collision energies are largely uncorrelated. Therefore, the sum of these in quadrature is taken as systematic uncertainty on the ratios. For both K^{*0} and ϕ, the differential yield ratio is independent of p_T within systematic uncertainties up to about 1 GeV/c for the different collision energies. This suggests that the particle production mechanism in soft scattering regions is independent of collision energy over the measured energy range. An increase in the slope of the differential yield ratios is observed for $p_T >$ 1–2 GeV/c.

TABLE II. Parameters extracted from the Lévy-Tsallis fit to the K^{*0} and ϕ transverse momentum spectra in inelastic pp collisions at $\sqrt{s} = 7$ and 8 TeV.

	pp, $\sqrt{s} = 8$ TeV		pp, $\sqrt{s} = 7$ TeV	
Particles	T (MeV)	n	T (MeV)	n
K^{*0}	260 ± 5	6.65 ± 0.03	261 ± 6	6.92 ± 0.15
ϕ	306 ± 6	7.28 ± 0.03	299 ± 5	7.17 ± 0.04

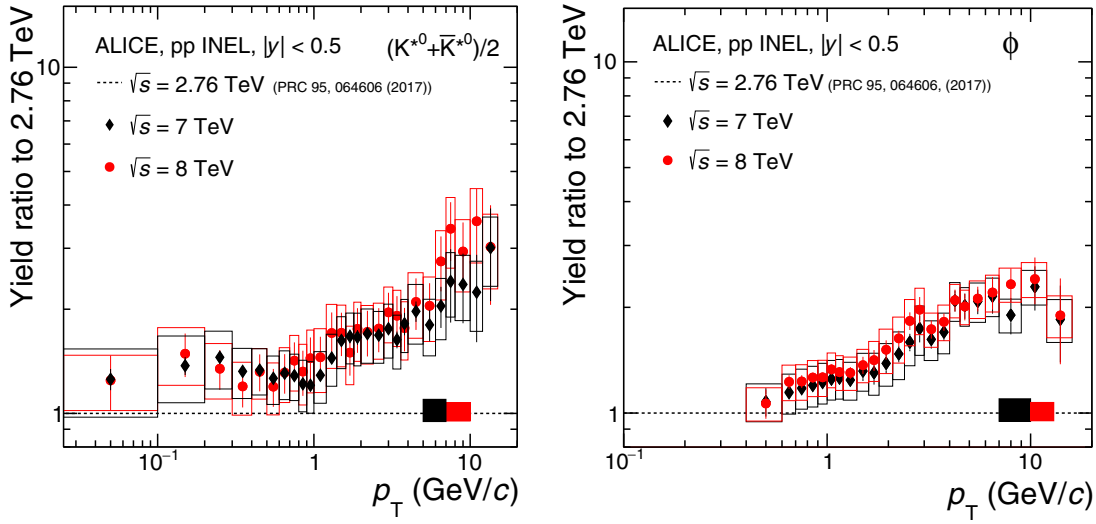

FIG. 3. Ratios of transverse-momentum spectra of K^{*0} and ϕ in inelastic events at $\sqrt{s} = 7$ and 8 TeV to the transverse-momentum spectra in pp collisions at $\sqrt{s} = 2.76$ TeV. The statistical and systematic uncertainties are shown as vertical error bars and boxes, respectively. The normalization uncertainties are indicated by boxes around unity.

B. p_{T}-integrated yields

Table III shows the K^{*0} and ϕ integrated yield (dN/dy) and mean transverse momenta ($\langle p_{\mathrm{T}} \rangle$) in inelastic pp collisions at $\sqrt{s} = 8$ TeV. As the ϕ spectrum starts from 0.4 GeV/c, for the calculation of dN/dy and $\langle p_{\mathrm{T}} \rangle$, the spectrum is extrapolated down to $p_{\mathrm{T}} = 0$ GeV/c using a Lévy-Tsallis fit [23,24]. The extrapolated part amounts to about 15% of the yield. Alternative fit functions (Boltzmann distribution, Bose-Einstein distribution, m_{T} exponential, and p_{T} exponential) have been tried for the extrapolation, giving a contribution of 1.5% to the total systematic uncertainty on dN/dy. In the case of K^{*0}, no extrapolation is needed as the distribution is measured for $p_{\mathrm{T}} > 0$ GeV/c. Table III also shows the dN/dy and $\langle p_{\mathrm{T}} \rangle$ of K^{*0} and ϕ at $\sqrt{s} = 7$ TeV.

C. Particle ratios

For the calculation of the particle yield ratios, the values of dN/dy for $\pi^+ + \pi^-$ and $K^+ + K^-$ in pp collisions at $\sqrt{s} = 8$ TeV are estimated via extrapolation by using the data points available at different LHC collision energies [10–12] namely 0.9, 2.76, and 7 TeV. The data points are fit with the polynomial function $A(\sqrt{s})^n + B$.

Here A, n, and B are the fit parameters. For the calculation of the uncertainties on the extrapolated value, the central values of the data points are shifted within their uncertainties and fit with the same function. The $\pi^+ + \pi^-$ and $K^+ + K^-$ energy extrapolated yields in inelastic pp collisions at $\sqrt{s} = 8$ TeV are 4.80 ± 0.21 and 0.614 ± 0.032. From here onwards, $\pi^+ + \pi^-$ is denoted as π and $K^+ + K^-$ is denoted as K.

Figure 4 shows the ratio of the dN/dy of K^{*0} (ϕ) to that of π in the left (right) panel, as a function of the collision energy. π has no strangeness content, K^{*0} has one unit of strangeness, and ϕ is strangeness neutral but contains two strange valence (anti)quarks. It is observed that the K^{*0}/π and ϕ/π ratios are independent of the collision energy within systematic uncertainties, which indicates that the chemistry of the system is independent of the energy from the RHIC to LHC energies. This also suggests that the strangeness

TABLE III. K^{*0} and ϕ integrated yields and $\langle p_{\mathrm{T}} \rangle$ in inelastic pp collisions at $\sqrt{s} = 7$ and 8 TeV. The systematic uncertainties include the contributions from the uncertainties listed in Table I and the choice of the spectrum fit function for extrapolation is also included for ϕ. Here, "stat." and "sys." refer to statistical and systematic uncertainties, respectively. In addition, dN/dy has uncertainties due to normalization, which is $^{+7.3}_{-3.5}$% for 7 TeV and 2.69% for 8 TeV.

pp, $\sqrt{s} = 8$ TeV			
Particles	measured p_{T} (GeV/c)	dN/dy	$\langle p_{\mathrm{T}} \rangle$ (GeV/c)
K^{*0}	0.0–20.0	0.101 ± 0.001 (stat.) ± 0.014 (sys.)	1.037 ± 0.006 (stat.) ± 0.029 (sys.)
ϕ	0.4–16.0	0.0335 ± 0.0003 (stat.) ± 0.0030 (sys.)	1.146 ± 0.005 (stat.) ± 0.040 (sys.)
pp, $\sqrt{s} = 7$ TeV			
Particles	measured p_{T} (GeV/c)	dN/dy	$\langle p_{\mathrm{T}} \rangle$ (GeV/c)
K^{*0}	0.0–20.0	0.0970 ± 0.0004 (stat.) ± 0.0103 (sys.)	1.015 ± 0.003 (stat.) ± 0.030 (sys.)
ϕ	0.4–21.0	0.0318 ± 0.0003 (stat.) ± 0.0032 (sys.)	1.132 ± 0.005 (stat.) ± 0.023 (sys.)

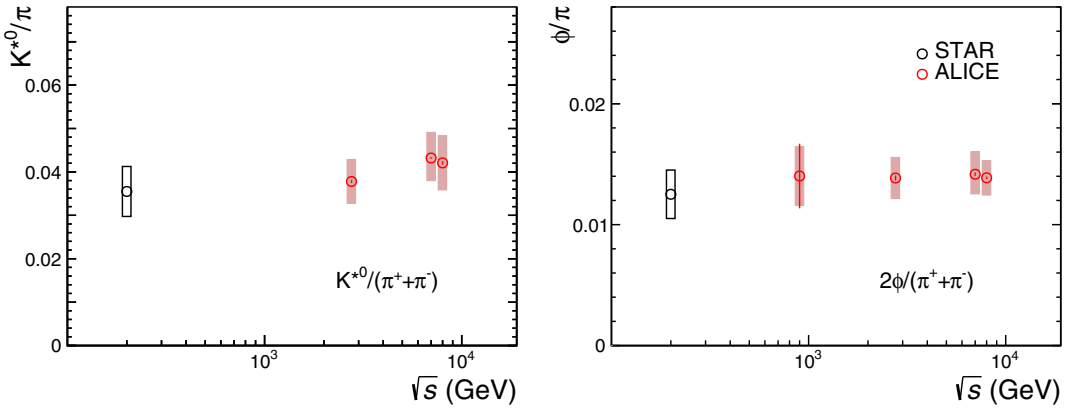

FIG. 4. Particle ratios of K^{*0}/π (left) and ϕ/π (right) are presented for pp collisions as a function of collision energy. Bars (when present) represent statistical uncertainties. Boxes represent the total systematic uncertainties or the total uncertainties for cases when separate statistical uncertainties were not reported [10–13,26,28–32].

production mechanisms do not depend on energy in inelastic pp collisions at LHC energies. Figure 4 and Ref. [13] show that this flat behavior is observed from BNL Relativistic Heavy Ion Collider (RHIC) to LHC energies and the new result at $\sqrt{s} = 8$ TeV is in agreement with previous findings. It is worth stressing that this flat behavior is not trivial: since particle yields do in fact increase with collision energy, the flat ratios are indicative of the fact that the percent increases of dN/dy for π, K^{*0}, and ϕ as a function of collision energy are similar from RHIC to LHC.

It is interesting to compare the particle ratios K^{*0}/K and ϕ/K measured in inelastic pp collisions with different collision systems and collision energies in order to understand the production dynamics. In Fig. 5 the K^{*0}/K and ϕ/K ratios are plotted as a function of center-of-mass energy per nucleon pair for different collision systems. The K^{*0}/K and ϕ/K ratios are independent of the collision energy and of the colliding system. The only exception is the K^{*0} in central nucleus-nucleus collisions; we attribute the suppression of the K^{*0}/K ratio to final-state effects in the late hadronic stage [26]. The behavior of these ratios in pp collisions agrees with the predictions [26,27] of a thermal model in the grand-canonical limit.

The ϕ/K^{*0} ratio as a function of center-of-mass energy is plotted in Fig. 6. The ratio seems to be independent of collision energy and appears to follow a behavior expected from the thermal production, within experimental uncertainties.

D. Comparison to models

QCD-inspired MC event generators like PYTHIA 8 [7], PHOJET [8,9], and EPOS-LHC [6] are used to study multiparticle production, which is predominantly a soft, nonperturbative process. The measurements are compared with the MC model predictions. PYTHIA 8 and PHOJET use the Lund string fragmentation model [42] for the hadronization of light and heavy quarks. We compare our data with the Monash 2013 tune [7] for PYTHIA 8, which is an updated parameter set for the Lund hadronization compared with previous tunes. To describe the nonperturbative phenomena (soft and semihard processes), PYTHIA 8 includes multiple parton-parton interactions while PHOJET uses the dual parton model [43]. For hard scatterings,

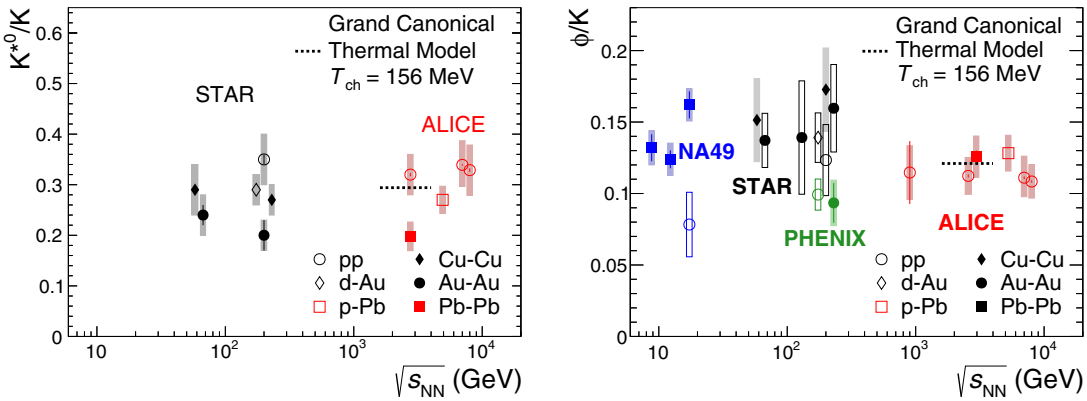

FIG. 5. Particle ratios of K^{*0}/K (left) and ϕ/K (right) are presented for pp, high-multiplicity p-Pb, central d-Au, and central A-A collisions [10–13,28–31,33–41] as a function of the collision energy. Bars (when present) represent statistical uncertainties. Boxes represent the total systematic uncertainties or the total uncertainties for cases when separate statistical uncertainties were not reported. The value given by a grand-canonical thermal model with a chemical freeze-out temperature of 156 MeV [27] is also shown.

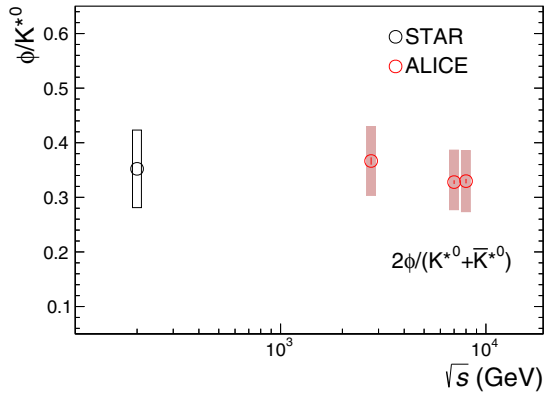

FIG. 6. Particle ratio ϕ/K^{*0} presented for pp collisions [13,26,28,29] as a function of collision energy. Bars (when present) represent statistical uncertainties. Boxes represent the total systematic uncertainties or the total uncertainties for cases when separate statistical uncertainties were not reported.

particle production in both models is based on perturbative QCD and only considers two-particle scatterings. For multiple scatterings, the EPOS-LHC model invokes Gribov's Reggeon field theory [44], which features a collective hadronization via the core-corona mechanism [45]. The final-state partonic system consists of longitudinal flux tubes which fragment into string segments. The high energy density string segments form the so-called "core" region, which evolves hydrodynamically to form the bulk part of the system in the final state. The low-density region is known as the "corona," which expands and breaks via the production of quark-antiquark pairs and hadronizes using vacuum string fragmentation. Recent data from the LHC have been used already to tune the EPOS-LHC model [6].

Figure 7 shows a comparison of the K^{*0} (left) and ϕ (right) p_{T} spectra in inelastic pp collisions with PYTHIA8, PHOJET, and EPOS-LHC. The bottom panels show the ratios of the p_{T} spectra from models to the p_{T} spectra measured by ALICE. The total fractional uncertainties from the real data, including both statistical and systematic uncertainties are shown as shaded boxes. PYTHIA 8 overestimates the p_{T} spectrum for K^{*0} at very low p_{T} but describes it in the intermediate-p_{T} region and approaches the experimental data at high p_{T}. For the ϕ meson, PYTHIA 8 underpredicts the yields from the experimental data by about a factor of two. PHOJET has a softer p_{T} spectrum for K^{*0} and it explains the data above $p_{\mathrm{T}} > 4$ GeV/c. For the ϕ meson, PHOJET predicts the yields similarly to PYTHIA 8 at low p_{T}, while it approaches the experimental data at higher p_{T}. For the K^{*0}, EPOS-LHC describes the p_{T} spectra at low p_{T} and overestimates the data above 4 GeV/c. For the ϕ meson, whereas PYTHIA and PHOJET fail to describe the p_{T} spectra, the EPOS-LHC model approaches the data at low p_{T} and deviates monotonically from them with increasing p_{T}.

V. CONCLUSIONS

Measurements of K^{*0} and ϕ production are presented at midrapidity in inelastic pp collisions at $\sqrt{s} = 8$ TeV in the range $0 < p_{\mathrm{T}} < 20$ GeV/c for K^{*0} and $0.4 < p_{\mathrm{T}} < 16$ GeV/c for ϕ. Also, updated measurements at $\sqrt{s} = 7$ TeV are presented, which improve the results previously published in Ref. [13]. In comparison with other LHC energies, a hardening of the p_{T} spectra is observed with increasing collision energy. The K^{*0}/π and ϕ/π ratios are independent of

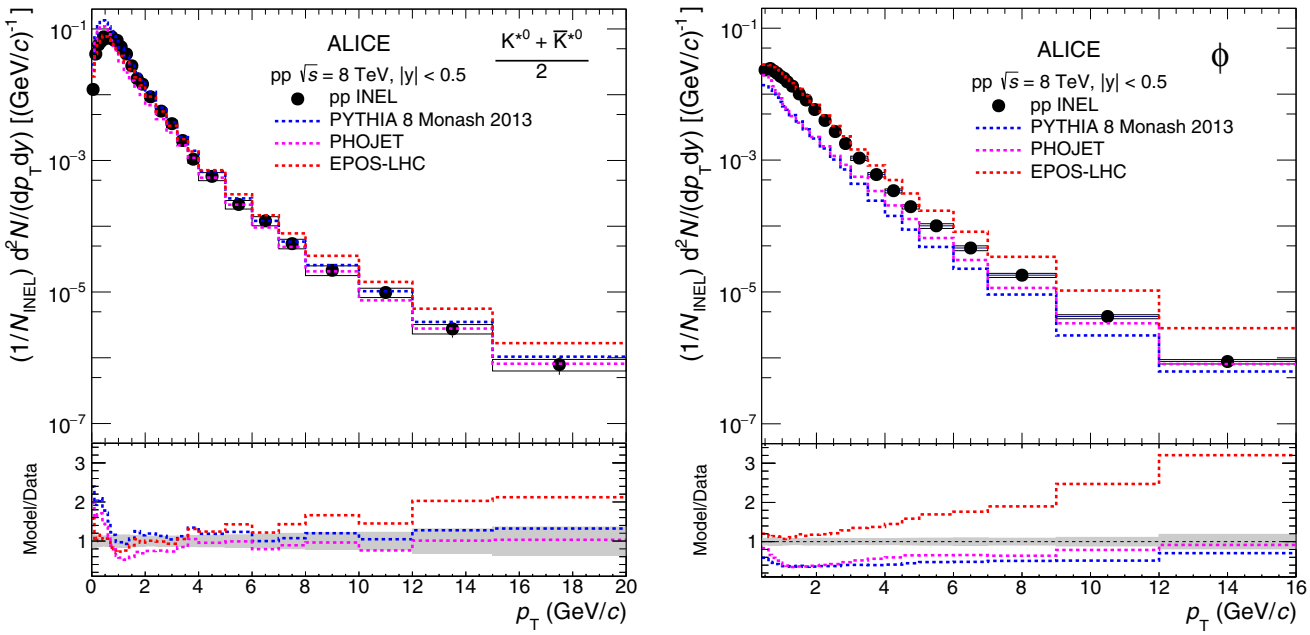

FIG. 7. Comparison of the K^{*0} (left) and ϕ (right) p_{T} spectra measured in inelastic pp collisions with those obtained from PYTHIA8 (Monash tune) [7], PHOJET [8,9] and EPOS-LHC [6]. The bottom plots show the ratios of the p_{T} spectra from the models to the measured p_{T} spectra by ALICE. The total fractional uncertainties of the data are shown as shaded boxes.

collision energy within systematic uncertainties. This indicates that there is no strangeness enhancement in inelastic pp collisions as the collision energy is increased. Similar behavior is observed for the K^{*0}/K and ϕ/K ratios as a function of collision energy. Also, no energy dependence of the ϕ/K^{*0} ratio in minimum-bias pp collisions at LHC energies is observed, which suggests there is no energy dependence of the chemistry of the system. None of the MC models seem to explain the K^{*0} spectra over the full p_{T} range whereas PHOJET and PYTHIA describe the data for the intermediate and high-p_{T} regions. However, the MC models fail to explain the p_{T} spectra of the ϕ meson completely. These pp results will serve as baseline for the measurements in p-Pb and Pb-Pb collisions.

ACKNOWLEDGMENTS

The ALICE Collaboration would like to thank all its engineers and technicians for their invaluable contributions to the construction of the experiment, and the CERN accelerator teams for the outstanding performance of the LHC complex. The ALICE Collaboration gratefully acknowledges the resources and support provided by all Grid centres and the Worldwide LHC Computing Grid (WLCG) collaboration. The ALICE Collaboration acknowledges the following funding agencies for their support in building and running the ALICE detector: A.I. Alikhanyan National Science Laboratory (Yerevan Physics Institute) Foundation (ANSL), State Committee of Science and World Federation of Scientists (WFS), Armenia; Austrian Academy of Sciences, Austrian Science Fund (FWF): [M 2467-N36] and Nationalstiftung für Forschung, Technologie und Entwicklung, Austria; Ministry of Communications and High Technologies, National Nuclear Research Center, Azerbaijan; Conselho Nacional de Desenvolvimento Científico e Tecnológico (CNPq), Universidade Federal do Rio Grande do Sul (UFRGS), Financiadora de Estudos e Projetos (Finep) and Fundação de Amparo à Pesquisa do Estado de São Paulo (FAPESP), Brazil; Ministry of Science & Technology of China (MSTC), National Natural Science Foundation of China (NSFC) and Ministry of Education of China (MOEC), China; Croatian Science Foundation and Ministry of Science and Education, Croatia; Centro de Aplicaciones Tecnológicas y Desarrollo Nuclear (CEADEN), Cubaenergía, Cuba; Ministry of Education, Youth and Sports of the Czech Republic, Czech Republic; The Danish Council for Independent Research | Natural Sciences, the Carlsberg Foundation and Danish National Research Foundation (DNRF), Denmark; Helsinki Institute of Physics (HIP), Finland; Commissariat à l'Energie Atomique (CEA), Institut National de Physique Nucléaire et de Physique des Particules (IN2P3) and Centre National de la Recherche Scientifique (CNRS) and Région des Pays de la Loire, France; Bundesministerium für Bildung und Forschung (BMBF) and GSI Helmholtzzentrum für Schwerionenforschung GmbH, Germany; General Secretariat for Research and Technology, Ministry of Education, Research and Religions, Greece; National Research, Development and Innovation Office, Hungary; Department of Atomic Energy Government of India (DAE), Department of Science and Technology, Government of India (DST), University Grants Commission, Government of India (UGC) and Council of Scientific and Industrial Research (CSIR), India; Indonesian Institute of Science, Indonesia; Centro Fermi - Museo Storico della Fisica e Centro Studi e Ricerche Enrico Fermi and Istituto Nazionale di Fisica Nucleare (INFN), Italy; Institute for Innovative Science and Technology, Nagasaki Institute of Applied Science (IIST), Japan Society for the Promotion of Science (JSPS) KAKENHI and Japanese Ministry of Education, Culture, Sports, Science and Technology (MEXT), Japan; Consejo Nacional de Ciencia (CONACYT) y Tecnología, through Fondo de Cooperación Internacional en Ciencia y Tecnología (FONCICYT) and Dirección General de Asuntos del Personal Academico (DGAPA), Mexico; Nederlandse Organisatie voor Wetenschappelijk Onderzoek (NWO), Netherlands; The Research Council of Norway, Norway; Commission on Science and Technology for Sustainable Development in the South (COMSATS), Pakistan; Pontificia Universidad Católica del Perú, Peru; Ministry of Science and Higher Education and National Science Centre, Poland; Korea Institute of Science and Technology Information and National Research Foundation of Korea (NRF), Republic of Korea; Ministry of Education and Scientific Research, Institute of Atomic Physics and Ministry of Research and Innovation and Institute of Atomic Physics, Romania; Joint Institute for Nuclear Research (JINR), Ministry of Education and Science of the Russian Federation, National Research Centre Kurchatov Institute, Russian Science Foundation and Russian Foundation for Basic Research, Russia; Ministry of Education, Science, Research and Sport of the Slovak Republic, Slovakia; National Research Foundation of South Africa, South Africa; Swedish Research Council (VR) and Knut & Alice Wallenberg Foundation (KAW), Sweden; European Organization for Nuclear Research, Switzerland; National Science and Technology Development Agency (NSDTA), Suranaree University of Technology (SUT) and Office of the Higher Education Commission under NRU project of Thailand, Thailand; Turkish Atomic Energy Agency (TAEK), Turkey; National Academy of Sciences of Ukraine, Ukraine; Science and Technology Facilities Council (STFC), United Kingdom; National Science Foundation of the United States of America (NSF) and United States Department of Energy, Office of Nuclear Physics (DOE NP), United States of America.

[1] J. C. Collins, D. E. Soper, and G. Sterman, Factorization of hard processes in QCD, *Perturbative QCD*, Advanced Series on Directions in High Energy Physics (World Scientific, Singapore, 1989), Vol. 5, pp. 1–91.

[2] D. de Florian, R. Sassot, M. Epele, R. J. Hernández-Pinto, and M. Stratmann, Parton-to-pion fragmentation reloaded, Phys. Rev. D **91**, 014035 (2015).

[3] D. de Florian, M. Epele, R. J. Hernandez-Pinto, R. Sassot, and M. Stratmann, Parton-to-kaon fragmentation revisited, Phys. Rev. D **95**, 094019 (2017).

[4] P. K. Malhotra and R. Orava, Measurement of strange quark suppression in hadronic vacuum, Z. Phys. C: Part. Fields **17**, 85 (1983).

[5] A. Wroblewski, On the strange quark suppression factor in high-energy collisions, Acta Phys. Polon. B **16**, 379 (1985).

[6] T. Pierog, I. Karpenko, J. M. Katzy, E. Yatsenko, and K. Werner, EPOS LHC: Test of collective hadronization with data measured at the CERN Large Hadron Collider, Phys. Rev. C **92**, 034906 (2015).

[7] P. Skands, S. Carrazza, and J. Rojo, Tuning PYTHIA 8.1: The Monash 2013 Tune, Eur. Phys. J. C **74**, 3024 (2014).

[8] R. Engel and J. Ranft, Hadronic photon-photon interactions at high-energies, Phys. Rev. D **54**, 4244 (1996).

[9] R. Engel, Photoproduction within the two component dual parton model : Amplitudes and cross-sections, Z. Phys. C: Part. Fields **66**, 203 (1995).

[10] K. Aamodt *et al.* (ALICE Collaboration), Production of pions, kaons and protons in pp collisions at $\sqrt{s} = 900$ GeV with ALICE at the LHC, Eur. Phys. J. C **71**, 1655 (2011).

[11] J. Adam *et al.* (ALICE Collaboration), Measurement of pion, kaon and proton production in proton-proton collisions at $\sqrt{s} =$ 7 TeV, Eur. Phys. J. C **75**, 226 (2015).

[12] B. Abelev *et al.* (ALICE Collaboration), Production of charged pions, kaons and protons at large transverse momenta in pp and Pb-Pb collisions at $\sqrt{s_{\rm NN}} = 2.76$ TeV, Phys. Lett. B **736**, 196 (2014).

[13] B. Abelev *et al.* (ALICE Collaboration), Production of $K^*(892)^0$ and $\phi(1020)$ in pp collisions at $\sqrt{s} = 7$ TeV, Eur. Phys. J. C **72**, 2183 (2012).

[14] K. Aamodt *et al.* (ALICE Collaboration), The ALICE experiment at the CERN LHC, J. Instrum. **3**, S08002 (2008).

[15] B. Abelev *et al.* (ALICE Collaboration), Performance of the ALICE Experiment at the CERN LHC, Int. J. Mod. Phys. A **29**, 1430044 (2014).

[16] M. Tanabashi *et al.* (Particle Data Group Collaboration), Review of particle physics, Phys. Rev. D **98**, 030001 (2018).

[17] C. Patrignani *et al.* (Particle Data Group Collaboration), Review of particle physics, Chin. Phys. C **40**, 100001 (2016).

[18] ALICE Collaboration, ALICE luminosity determination for pp collisions at $\sqrt{s} = 8$ TeV; https://cds.cern.ch/record/2255216

[19] C. Loizides, J. Kamin, and D. d'Enterria, Improved Monte Carlo Glauber predictions at present and future nuclear colliders, Phys. Rev. C **97**, 054910 (2018); **99**, 019901(E) (2019).

[20] R. Brun, R. Hagelberg, M. Hansroul, and J. C. Lassalle, Geant: Simulation Program for Particle Physics Experiments. User Guide and Reference Manual, CERN-DD-78-2-REV, CERN-DD-78-2 (1978).

[21] B. Abelev *et al.* (ALICE Collaboration), Centrality dependence of π, K, p production in Pb-Pb collisions at $\sqrt{s_{NN}} = 2.76$ TeV, Phys. Rev. C **88**, 044910 (2013).

[22] B. Abelev *et al.* (ALICE Collaboration), Multiplicity dependence of pion, kaon, proton and lambda production in p-Pb collisions at $\sqrt{s_{NN}} = 5.02$ TeV, Phys. Lett. B **728**, 25 (2014).

[23] C. Tsallis, Possible generalization of Boltzmann-Gibbs statistics, J. Stat. Phys. **52**, 479 (1988).

[24] B. I. Abelev *et al.* (STAR Collaboration), Strange particle production in $p + p$ collisions at $\sqrt{s} = 200$ GeV, Phys. Rev. C **75**, 064901 (2007).

[25] J. Adam *et al.* (ALICE Collaboration), $K^*(892)^0$ and $\phi(1020)$ meson production at high transverse momentum in pp and Pb-Pb collisions at $\sqrt{s_{\rm NN}} = 2.76$ TeV, Phys. Rev. C **95**, 064606 (2017).

[26] B. Abelev *et al.* (ALICE Collaboration), $K^*(892)^0$ and $\phi(1020)$ production in Pb-Pb collisions at $\sqrt{s_{NN}} = 2.76$ TeV, Phys. Rev. C **91**, 024609 (2015).

[27] J. Stachel, A. Andronic, P. Braun-Munzinger, and K. Redlich, Confronting LHC data with the statistical hadronization model, J. Phys.: Conf. Ser. **509**, 012019 (2014).

[28] J. Adams *et al.* (STAR Collaboration), K(892)* resonance production in Au + Au and $p + p$ collisions at $\sqrt{s_{NN}} = 200$ GeV at STAR, Phys. Rev. C **71**, 064902 (2005).

[29] J. Adams *et al.* (STAR Collaboration), ϕ meson production in Au + Au and $p + p$ collisions at $\sqrt{s_{NN}} = 200$ GeV, Phys. Lett. B **612**, 181 (2005).

[30] K. Aamodt *et al.* (ALICE Collaboration), Strange particle production in proton-proton collisions at $\sqrt{s} = 0.9$ TeV with ALICE at the LHC, Eur. Phys. J. C **71**, 1594 (2011).

[31] B. I. Abelev *et al.* (STAR Collaboration), Measurements of ϕ meson production in relativistic heavy-ion collisions at RHIC, Phys. Rev. C **79**, 064903 (2009).

[32] J. Adams *et al.* (STAR Collaboration), Identified Particle Distributions in pp and Au + Au Collisions at $\sqrt{s_{NN}} = 200$ GeV, Phys. Rev. Lett. **92**, 112301 (2004).

[33] S. S. Adler *et al.* (PHENIX Collaboration), Production of ϕ mesons at mid-rapidity in $\sqrt{s_{NN}} = 200$ GeV Au + Au collisions at RHIC, Phys. Rev. C **72**, 014903 (2005).

[34] M. M. Aggarwal *et al.* (STAR Collaboration), K^{*0} production in Cu + Cu and Au + Au collisions at $\sqrt{s_{NN}} = 62.4$ GeV and 200 GeV, Phys. Rev. C **84**, 034909 (2011).

[35] C. Alt *et al.* (NA49 Collaboration), Energy dependence of ϕ meson production in central Pb + Pb collisions at $\sqrt{s_{NN}} = 6$ to 17 GeV, Phys. Rev. C **78**, 044907 (2008).

[36] B. I. Abelev *et al.* (STAR Collaboration), Hadronic resonance production in d + Au collisions at $\sqrt{s_{NN}} = 200$ GeV at RHIC, Phys. Rev. C **78**, 044906 (2008).

[37] S. V. Afanasiev *et al.* (NA49 Collaboration), Production of ϕ mesons in $p + p$, p + Pb and central Pb + Pb collisions at $E_{\rm beam} = 158A$ GeV, Phys. Lett. B **491**, 59 (2000).

[38] S. V. Afanasiev *et al.* (NA49 Collaboration), Energy dependence of pion and kaon production in central Pb + Pb collisions, Phys. Rev. C **66**, 054902 (2002).

[39] C. Adler *et al.* (STAR Collaboration), Midrapidity ϕ production in Au + Au collisions at $\sqrt{s_{NN}} = 130$ GeV, Phys. Rev. C **65**, 041901 (2002).

[40] A. Adare *et al.* (PHENIX Collaboration), Measurement of neutral mesons in $p + p$ collisions at $\sqrt{s} = 200$ GeV and scaling properties of hadron production, Phys. Rev. D **83**, 052004 (2011).

[41] A. Adare *et al.* (PHENIX Collaboration), Identified charged hadron production in $p + p$ collisions at $\sqrt{s} = 200$ and 62.4 GeV, Phys. Rev. C **83**, 064903 (2011).

[42] B. Andersson, G. Gustafson, G. Ingelman, and T. Sjöstrand, Parton fragmentation and string dynamics, Phys. Rep. **97**, 31 (1983).

[43] A. Capella, U. Sukhatme, C.-I. Tan, and J. Tran Thanh Van, Dual parton model, Phys. Rep. **236**, 225 (1994).

[44] G. A. Schuler and T. Sjöstrand, Hadronic diffractive cross-sections and the rise of the total cross section, Phys. Rev. D **49**, 2257 (1994).

[45] K. Werner, Core-Corona Separation in Ultra-Relativistic Heavy Ion Collisions, Phys. Rev. Lett. **98**, 152301 (2007).

S. Acharya,[141] D. Adamová,[93] S. P. Adhya,[141] A. Adler,[73] J. Adolfsson,[79] M. M. Aggarwal,[98] G. Aglieri Rinella,[34] M. Agnello,[31] N. Agrawal,[10,48,53] Z. Ahammed,[141] S. Ahmad,[17] S. U. Ahn,[75] A. Akindinov,[90] M. Al-Turany,[105] S. N. Alam,[141] D. S. D. Albuquerque,[122] D. Aleksandrov,[86] B. Alessandro,[58] H. M. Alfanda,[6] R. Alfaro Molina,[71] B. Ali,[17] Y. Ali,[15] A. Alici,[10,27,53] A. Alkin,[2] J. Alme,[22] T. Alt,[68] L. Altenkamper,[22] I. Altsybeev,[112] M. N. Anaam,[6] C. Andrei,[47] D. Andreou,[34] H. A. Andrews,[109] A. Andronic,[144] M. Angeletti,[34] V. Anguelov,[102] C. Anson,[16] T. Antičić,[106] F. Antinori,[56] P. Antonioli,[53] R. Anwar,[125] N. Apadula,[78] L. Aphecetche,[114] H. Appelshäuser,[68] S. Arcelli,[27] R. Arnaldi,[58] M. Arratia,[78] I. C. Arsene,[21] M. Arslandok,[102] A. Augustinus,[34] R. Averbeck,[105] S. Aziz,[61] M. D. Azmi,[17] A. Badalà,[55] Y. W. Baek,[40] S. Bagnasco,[58] X. Bai,[105] R. Bailhache,[68] R. Bala,[99] A. Baldisseri,[137] M. Ball,[42] S. Balouza,[103] R. C. Baral,[84] R. Barbera,[28] L. Barioglio,[26] G. G. Barnaföldi,[145] L. S. Barnby,[92] V. Barret,[134] P. Bartalini,[6] K. Barth,[34] E. Bartsch,[68] F. Baruffaldi,[29] N. Bastid,[134] S. Basu,[143] G. Batigne,[114] B. Batyunya,[74] P. C. Batzing,[21] D. Bauri,[48] J. L. Bazo Alba,[110] I. G. Bearden,[87] C. Bedda,[63] N. K. Behera,[60] I. Belikov,[136] F. Bellini,[34] R. Bellwied,[125] V. Belyaev,[91] G. Bencedi,[145] S. Beole,[26] A. Bercuci,[47] Y. Berdnikov,[96] D. Berenyi,[145] R. A. Bertens,[130] D. Berzano,[58] M. G. Besoiu,[67] L. Betev,[34] A. Bhasin,[99] I. R. Bhat,[99] M. A. Bhat,[3] H. Bhatt,[48] B. Bhattacharjee,[41] A. Bianchi,[26] L. Bianchi,[26] N. Bianchi,[51] J. Bielčík,[37] J. Bielčíková,[93] A. Bilandzic,[103,117] G. Biro,[145] R. Biswas,[3] S. Biswas,[3] J. T. Blair,[119] D. Blau,[86] C. Blume,[68] G. Boca,[139] F. Bock,[34,94] A. Bogdanov,[91] L. Boldizsár,[145] A. Bolozdynya,[91] M. Bombara,[38] G. Bonomi,[140] H. Borel,[137] A. Borissov,[91,144] M. Borri,[127] H. Bossi,[146] E. Botta,[26] L. Bratrud,[68] P. Braun-Munzinger,[105] M. Bregant,[121] T. A. Broker,[68] M. Broz,[37] E. J. Brucken,[43] E. Bruna,[58] G. E. Bruno,[33,104] M. D. Buckland,[127] D. Budnikov,[107] H. Buesching,[68] S. Bufalino,[31] O. Bugnon,[114] P. Buhler,[113] P. Buncic,[34] Z. Buthelezi,[72] J. B. Butt,[15] J. T. Buxton,[95] S. A. Bysiak,[118] D. Caffarri,[88] A. Caliva,[105] E. Calvo Villar,[110] R. S. Camacho,[44] P. Camerini,[25] A. A. Capon,[113] F. Carnesecchi,[10] J. Castillo Castellanos,[137] A. J. Castro,[130] E. A. R. Casula,[54] F. Catalano,[31] C. Ceballos Sanchez,[52] P. Chakraborty,[48] S. Chandra,[141] B. Chang,[126] W. Chang,[6] S. Chapeland,[34] M. Chartier,[127] S. Chattopadhyay,[141] S. Chattopadhyay,[108] A. Chauvin,[24] C. Cheshkov,[135] B. Cheynis,[135] V. Chibante Barroso,[34] D. D. Chinellato,[122] S. Cho,[60] P. Chochula,[34] T. Chowdhury,[134] P. Christakoglou,[88] C. H. Christensen,[87] P. Christiansen,[79] T. Chujo,[133] C. Cicalo,[54] L. Cifarelli,[10,27] F. Cindolo,[53] J. Cleymans,[124] F. Colamaria,[52] D. Colella,[52] A. Collu,[78] M. Colocci,[27] M. Concas,[58,a] G. Conesa Balbastre,[77] Z. Conesa del Valle,[61] G. Contin,[59,127] J. G. Contreras,[37] T. M. Cormier,[94] Y. Corrales Morales,[26,58] P. Cortese,[32] M. R. Cosentino,[123] F. Costa,[34] S. Costanza,[139] J. Crkovská,[61] P. Crochet,[134] E. Cuautle,[69] L. Cunqueiro,[94] D. Dabrowski,[142] T. Dahms,[103,117] A. Dainese,[56] F. P. A. Damas,[114,137] S. Dani,[65] M. C. Danisch,[102] A. Danu,[67] D. Das,[108] I. Das,[108] P. Das,[3] S. Das,[3] A. Dash,[84] S. Dash,[48] A. Dashi,[103] S. De,[49,84] A. De Caro,[30] G. de Cataldo,[52] C. de Conti,[121] J. de Cuveland,[39] A. De Falco,[24] D. De Gruttola,[10] N. De Marco,[58] S. De Pasquale,[30] R. D. De Souza,[122] S. Deb,[49] H. F. Degenhardt,[121] K. R. Deja,[142] A. Deloff,[83] S. Delsanto,[26,131] D. Devetak,[105] P. Dhankher,[48] D. Di Bari,[33] A. Di Mauro,[34] R. A. Diaz,[8] T. Dietel,[124] P. Dillenseger,[68] Y. Ding,[6] R. Divià,[34] Ø. Djuvsland,[22] U. Dmitrieva,[62] A. Dobrin,[34,67] B. Dönigus,[68] O. Dordic,[21] A. K. Dubey,[141] A. Dubla,[105] S. Dudi,[98] M. Dukhishyam,[84] P. Dupieux,[134] R. J. Ehlers,[146] D. Elia,[52] H. Engel,[73] E. Epple,[146] B. Erazmus,[114] F. Erhardt,[97] A. Erokhin,[112] M. R. Ersdal,[22] B. Espagnon,[61] G. Eulisse,[34] J. Eum,[18] D. Evans,[109] S. Evdokimov,[89] L. Fabbietti,[103,117] M. Faggin,[29] J. Faivre,[77] A. Fantoni,[51] M. Fasel,[94] P. Fecchio,[31] A. Feliciello,[58] G. Feofilov,[112] A. Fernández Téllez,[44] A. Ferrero,[137] A. Ferretti,[26] A. Festanti,[34] V. J. G. Feuillard,[102] J. Figiel,[118] S. Filchagin,[107] D. Finogeev,[62] F. M. Fionda,[22] G. Fiorenza,[52] F. Flor,[125] S. Foertsch,[72] P. Foka,[105] S. Fokin,[86] E. Fragiacomo,[59] U. Frankenfeld,[105] G. G. Fronze,[26] U. Fuchs,[34] C. Furget,[77] A. Furs,[62] M. Fusco Girard,[30] J. J. Gaardhøje,[87] M. Gagliardi,[26] A. M. Gago,[110] A. Gal,[136] C. D. Galvan,[120] P. Ganoti,[82] C. Garabatos,[105] E. Garcia-Solis,[11] K. Garg,[28] C. Gargiulo,[34] A. Garibli,[85] K. Garner,[144] P. Gasik,[103,117] E. F. Gauger,[119] M. B. Gay Ducati,[70] M. Germain,[114] J. Ghosh,[108] P. Ghosh,[141] S. K. Ghosh,[3] P. Gianotti,[51] P. Giubellino,[58,105] P. Giubilato,[29] P. Glässel,[102] D. M. Goméz Coral,[71] A. Gomez Ramirez,[73] V. Gonzalez,[105] P. González-Zamora,[44] S. Gorbunov,[39] L. Görlich,[118] S. Gotovac,[35] V. Grabski,[71] L. K. Graczykowski,[142] K. L. Graham,[109] L. Greiner,[78] A. Grelli,[63] C. Grigoras,[34] V. Grigoriev,[91] A. Grigoryan,[1] S. Grigoryan,[74] O. S. Groettvik,[22] J. M. Gronefeld,[105] F. Grosa,[31] J. F. Grosse-Oetringhaus,[34] R. Grosso,[105] R. Guernane,[77] B. Guerzoni,[27] M. Guittiere,[114] K. Gulbrandsen,[87] T. Gunji,[132] A. Gupta,[99] R. Gupta,[99] I. B. Guzman,[44] R. Haake,[146] M. K. Habib,[105] C. Hadjidakis,[61] H. Hamagaki,[80] G. Hamar,[145] M. Hamid,[6] R. Hannigan,[119] M. R. Haque,[63] A. Harlenderova,[105] J. W. Harris,[146] A. Harton,[11] J. A. Hasenbichler,[34] H. Hassan,[77] D. Hatzifotiadou,[10,53] P. Hauer,[42] S. Hayashi,[132] A. D. L. B. Hechavarria,[144] S. T. Heckel,[68] E. Hellbär,[68] H. Helstrup,[36] A. Herghelegiu,[47] E. G. Hernandez,[44] G. Herrera Corral,[9] F. Herrmann,[144] K. F. Hetland,[36] T. E. Hilden,[43] H. Hillemanns,[34] C. Hills,[127] B. Hippolyte,[136] B. Hohlweger,[103] D. Horak,[37] S. Hornung,[105] R. Hosokawa,[133] P. Hristov,[34] C. Huang,[61] C. Hughes,[130] P. Huhn,[68] T. J. Humanic,[95] H. Hushnud,[108] L. A. Husova,[144] N. Hussain,[41] S. A. Hussain,[15] T. Hussain,[17] D. Hutter,[39] D. S. Hwang,[19] J. P. Iddon,[34,127] R. Ilkaev,[107] M. Inaba,[133] M. Ippolitov,[86] M. S. Islam,[108] M. Ivanov,[105] V. Ivanov,[96] V. Izucheev,[89] B. Jacak,[78] N. Jacazio,[27] P. M. Jacobs,[78] M. B. Jadhav,[48] S. Jadlovska,[116] J. Jadlovsky,[116] S. Jaelani,[63] C. Jahnke,[121] M. J. Jakubowska,[142] M. A. Janik,[142] M. Jercic,[97] O. Jevons,[109] R. T. Jimenez Bustamante,[105] M. Jin,[125] F. Jonas,[94,144] P. G. Jones,[109] J. Jung,[68] M. Jung,[68] A. Jusko,[109] P. Kalinak,[64] A. Kalweit,[34] J. H. Kang,[147] V. Kaplin,[91] S. Kar,[6] A. Karasu Uysal,[76] O. Karavichev,[62] T. Karavicheva,[62] P. Karczmarczyk,[34] E. Karpechev,[62] U. Kebschull,[73] R. Keidel,[46] M. Keil,[34] B. Ketzer,[42] Z. Khabanova,[88] A. M. Khan,[6] S. Khan,[17] S. A. Khan,[141] A. Khanzadeev,[96] Y. Kharlov,[89] A. Khatun,[17] A. Khuntia,[49,118] B. Kileng,[36] B. Kim,[60] B. Kim,[133] D. Kim,[147] D. J. Kim,[126] E. J. Kim,[13] H. Kim,[147] J. Kim,[147] J. S. Kim,[40] J. Kim,[102] J. Kim,[147] J. Kim,[13] M. Kim,[102] S. Kim,[19] T. Kim,[147] T. Kim,[147] S. Kirsch,[39] I. Kisel,[39] S. Kiselev,[90] A. Kisiel,[142] J. L. Klay,[5] C. Klein,[68] J. Klein,[58] S. Klein,[78] C. Klein-Bösing,[144] S. Klewin,[102] A. Kluge,[34] M. L. Knichel,[34] A. G. Knospe,[125] C. Kobdaj,[115] M. K. Köhler,[102]

T. Kollegger,[105] A. Kondratyev,[74] N. Kondratyeva,[91] E. Kondratyuk,[89] P. J. Konopka,[34] L. Koska,[116] O. Kovalenko,[83] V. Kovalenko,[112] M. Kowalski,[118] I. Králik,[64] A. Kravčáková,[38] L. Kreis,[105] M. Krivda,[64,109] F. Krizek,[93] K. Krizkova Gajdosova,[37] M. Krüger,[68] E. Kryshen,[96] M. Krzewicki,[39] A. M. Kubera,[95] V. Kučera,[60] C. Kuhn,[136] P. G. Kuijer,[88] L. Kumar,[98] S. Kumar,[48] S. Kundu,[84] P. Kurashvili,[83] A. Kurepin,[62] A. B. Kurepin,[62] A. Kuryakin,[107] S. Kushpil,[93] J. Kvapil,[109] M. J. Kweon,[60] J. Y. Kwon,[60] Y. Kwon,[147] S. L. La Pointe,[39] P. La Rocca,[28] Y. S. Lai,[78] R. Langoy,[129] K. Lapidus,[34,146] A. Lardeux,[21] P. Larionov,[51] E. Laudi,[34] R. Lavicka,[37] T. Lazareva,[112] R. Lea,[25] L. Leardini,[102] S. Lee,[147] F. Lehas,[88] S. Lehner,[113] J. Lehrbach,[39] R. C. Lemmon,[92] I. León Monzón,[120] E. D. Lesser,[20] M. Lettrich,[34] P. Lévai,[145] X. Li,[12] X. L. Li,[6] J. Lien,[129] R. Lietava,[109] B. Lim,[18] S. Lindal,[21] V. Lindenstruth,[39] S. W. Lindsay,[127] C. Lippmann,[105] M. A. Lisa,[95] V. Litichevskyi,[43] A. Liu,[78] S. Liu,[95] W. J. Llope,[143] I. M. Lofnes,[22] V. Loginov,[91] C. Loizides,[94] P. Loncar,[35] X. Lopez,[134] E. López Torres,[8] P. Luettig,[68] J. R. Luhder,[144] M. Lunardon,[29] G. Luparello,[59] M. Lupi,[73] A. Maevskaya,[62] M. Mager,[34] S. M. Mahmood,[21] T. Mahmoud,[42] A. Maire,[136] R. D. Majka,[146] M. Malaev,[96] Q. W. Malik,[21] L. Malinina,[74,b] D. Mal'Kevich,[90] P. Malzacher,[105] A. Mamonov,[107] G. Mandaglio,[55] V. Manko,[86] F. Manso,[134] V. Manzari,[52] Y. Mao,[6] M. Marchisone,[135] J. Mareš,[66] G. V. Margagliotti,[25] A. Margotti,[53] J. Margutti,[63] A. Marín,[105] C. Markert,[119] M. Marquard,[68] N. A. Martin,[102] P. Martinengo,[34] J. L. Martinez,[125] M. I. Martínez,[44] G. Martínez García,[114] M. Martinez Pedreira,[34] S. Masciocchi,[105] M. Masera,[26] A. Masoni,[54] L. Massacrier,[61] E. Masson,[114] A. Mastroserio,[138] A. M. Mathis,[103,117] O. Matonoha,[79] P. F. T. Matuoka,[121] A. Matyja,[118] C. Mayer,[118] M. Mazzilli,[33] M. A. Mazzoni,[57] A. F. Mechler,[68] F. Meddi,[23] Y. Melikyan,[91] A. Menchaca-Rocha,[71] E. Meninno,[30] M. Meres,[14] S. Mhlanga,[124] Y. Miake,[133] L. Micheletti,[26] M. M. Mieskolainen,[43] D. L. Mihaylov,[103] K. Mikhaylov,[74,90] A. Mischke,[63,c] A. N. Mishra,[69] D. Miśkowiec,[105] C. M. Mitu,[67] A. Modak,[3] N. Mohammadi,[34] A. P. Mohanty,[63] B. Mohanty,[84] M. Mohisin Khan,[17,d] M. Mondal,[141] M. M. Mondal,[65] C. Mordasini,[103] D. A. Moreira De Godoy,[144] L. A. P. Moreno,[44] S. Moretto,[29] A. Morreale,[114] A. Morsch,[34] T. Mrnjavac,[34] V. Muccifora,[51] E. Mudnic,[35] D. Mühlheim,[144] S. Muhuri,[141] J. D. Mulligan,[78] M. G. Munhoz,[121] K. Münning,[42] R. H. Munzer,[68] H. Murakami,[132] S. Murray,[72] L. Musa,[34] J. Musinsky,[64] C. J. Myers,[125] J. W. Myrcha,[142] B. Naik,[48] R. Nair,[83] B. K. Nandi,[48] R. Nania,[10,53] E. Nappi,[52] M. U. Naru,[15] A. F. Nassirpour,[79] H. Natal da Luz,[121] C. Nattrass,[130] R. Nayak,[48] T. K. Nayak,[84,141] S. Nazarenko,[107] R. A. Negrao De Oliveira,[68] L. Nellen,[69] S. V. Nesbo,[36] G. Neskovic,[39] B. S. Nielsen,[87] S. Nikolaev,[86] S. Nikulin,[86] V. Nikulin,[96] F. Noferini,[10,53] P. Nomokonov,[74] G. Nooren,[63] J. Norman,[77] N. Novitzky,[133] P. Nowakowski,[142] A. Nyanin,[86] J. Nystrand,[22] M. Ogino,[80] A. Ohlson,[102] J. Oleniacz,[142] A. C. Oliveira Da Silva,[121] M. H. Oliver,[146] C. Oppedisano,[58] R. Orava,[43] A. Ortiz Velasquez,[69] A. Oskarsson,[79] J. Otwinowski,[118] K. Oyama,[80] Y. Pachmayer,[102] V. Pacik,[87] D. Pagano,[140] G. Paić,[69] P. Palni,[6] J. Pan,[143] A. K. Pandey,[48] S. Panebianco,[137] V. Papikyan,[1] P. Pareek,[49] J. Park,[60] J. E. Parkkila,[126] S. Parmar,[98] A. Passfeld,[144] S. P. Pathak,[125] R. N. Patra,[141] B. Paul,[24,58] H. Pei,[6] T. Peitzmann,[63] X. Peng,[6] L. G. Pereira,[70] H. Pereira Da Costa,[137] D. Peresunko,[86] G. M. Perez,[8] E. Perez Lezama,[68] V. Peskov,[68] Y. Pestov,[4] V. Petráček,[37] M. Petrovici,[47] R. P. Pezzi,[70] S. Piano,[59] M. Pikna,[14] P. Pillot,[114] L. O. D. L. Pimentel,[87] O. Pinazza,[34,53] L. Pinsky,[125] C. Pinto,[28] S. Pisano,[51] D. B. Piyarathna,[125] M. Płoskoń,[78] M. Planinic,[97] F. Pliquett,[68] J. Pluta,[142] S. Pochybova,[145] M. G. Poghosyan,[94] B. Polichtchouk,[89] N. Poljak,[97] W. Poonsawat,[115] A. Pop,[47] H. Poppenborg,[144] S. Porteboeuf-Houssais,[134] V. Pozdniakov,[74] S. K. Prasad,[3] R. Preghenella,[53] F. Prino,[58] C. A. Pruneau,[143] I. Pshenichnov,[62] M. Puccio,[26,34] V. Punin,[107] K. Puranapanda,[141] J. Putschke,[143] R. E. Quishpe,[125] S. Ragoni,[109] S. Raha,[3] S. Rajput,[99] J. Rak,[126] A. Rakotozafindrabe,[137] L. Ramello,[32] F. Rami,[136] R. Raniwala,[100] S. Raniwala,[100] S. S. Räsänen,[43] B. T. Rascanu,[68] R. Rath,[49] V. Ratza,[42] I. Ravasenga,[31] K. F. Read,[94,130] K. Redlich,[83,e] A. Rehman,[22] P. Reichelt,[68] F. Reidt,[34] X. Ren,[6] R. Renfordt,[68] A. Reshetin,[62] J.-P. Revol,[10] K. Reygers,[102] V. Riabov,[96] T. Richert,[79,87] M. Richter,[21] P. Riedler,[34] W. Riegler,[34] F. Riggi,[28] C. Ristea,[67] S. P. Rode,[49] M. Rodríguez Cahuantzi,[44] K. Røed,[21] R. Rogalev,[89] E. Rogochaya,[74] D. Rohr,[34] D. Röhrich,[22] P. S. Rokita,[142] F. Ronchetti,[51] E. D. Rosas,[69] K. Roslon,[142] P. Rosnet,[134] A. Rossi,[29] A. Rotondi,[139] F. Roukoutakis,[82] A. Roy,[49] P. Roy,[108] O.V. Rueda,[79] R. Rui,[25] B. Rumyantsev,[74] A. Rustamov,[85] E. Ryabinkin,[86] Y. Ryabov,[96] A. Rybicki,[118] H. Rytkonen,[126] S. Sadhu,[141] S. Sadovsky,[89] K. Šafařík,[34,37] S. K. Saha,[141] B. Sahoo,[48] P. Sahoo,[48,49] R. Sahoo,[49] S. Sahoo,[65] P. K. Sahu,[65] J. Saini,[141] S. Sakai,[133] S. Sambyal,[99] V. Samsonov,[91,96] F. R. Sanchez,[44] A. Sandoval,[71] A. Sarkar,[72] D. Sarkar,[143] N. Sarkar,[141] P. Sarma,[41] V. M. Sarti,[103] M. H. P. Sas,[63] E. Scapparone,[53] B. Schaefer,[94] J. Schambach,[119] H. S. Scheid,[68] C. Schiaua,[47] R. Schicker,[102] A. Schmah,[102] C. Schmidt,[105] H. R. Schmidt,[101] M. O. Schmidt,[102] M. Schmidt,[101] N. V. Schmidt,[68,94] A. R. Schmier,[130] J. Schukraft,[34,87] Y. Schutz,[34,136] K. Schwarz,[105] K. Schweda,[105] G. Scioli,[27] E. Scomparin,[58] M. Šefčík,[38] J. E. Seger,[16] Y. Sekiguchi,[132] D. Sekihata,[45,132] I. Selyuzhenkov,[91,105] S. Senyukov,[136] D. Serebryakov,[62] E. Serradilla,[71] P. Sett,[48] A. Sevcenco,[67] A. Shabanov,[62] A. Shabetai,[114] R. Shahoyan,[34] W. Shaikh,[108] A. Shangaraev,[89] A. Sharma,[98] A. Sharma,[99] H. Sharma,[118] M. Sharma,[99] N. Sharma,[98] A. I. Sheikh,[141] K. Shigaki,[45] M. Shimomura,[81] S. Shirinkin,[90] Q. Shou,[111] Y. Sibiriak,[86] S. Siddhanta,[54] T. Siemiarczuk,[83] D. Silvermyr,[79] C. Silvestre,[77] G. Simatovic,[88] G. Simonetti,[34,103] R. Singh,[84] R. Singh,[99] V. K. Singh,[141] V. Singhal,[141] T. Sinha,[108] B. Sitar,[14] M. Sitta,[32] T. B. Skaali,[21] M. Slupecki,[126] N. Smirnov,[146] R. J. M. Snellings,[63] T. W. Snellman,[126] J. Sochan,[116] C. Soncco,[110] J. Song,[60,125] A. Songmoolnak,[115] F. Soramel,[29] S. Sorensen,[130] I. Sputowska,[118] J. Stachel,[102] I. Stan,[67] P. Stankus,[94] P. J. Steffanic,[130] E. Stenlund,[79] D. Stocco,[114] M. M. Storetvedt,[36] P. Strmen,[14] A. A. P. Suaide,[121] T. Sugitate,[45] C. Suire,[61] M. Suleymanov,[15] M. Suljic,[34] R. Sultanov,[90] M. Šumbera,[93] S. Sumowidagdo,[50] K. Suzuki,[113] S. Swain,[65] A. Szabo,[14] I. Szarka,[14] U. Tabassam,[15] G. Taillepied,[134] J. Takahashi,[122] G. J. Tambave,[22] S. Tang,[6,134] M. Tarhini,[114] M. G. Tarzila,[47] A. Tauro,[34] G. Tejeda Muñoz,[44] A. Telesca,[34] C. Terrevoli,[29,125] D. Thakur,[49] S. Thakur,[141] D. Thomas,[119] F. Thoresen,[87] R. Tieulent,[135] A. Tikhonov,[62] A. R. Timmins,[125] A. Toia,[68] N. Topilskaya,[62] M. Toppi,[51] F. Torales-Acosta,[20] S. R. Torres,[120]

A. Trifiro,[55] S. Tripathy,[49] T. Tripathy,[48] S. Trogolo,[26,29] G. Trombetta,[33] L. Tropp,[38] V. Trubnikov,[2] W. H. Trzaska,[126] T. P. Trzcinski,[142] B. A. Trzeciak,[63] T. Tsuji,[132] A. Tumkin,[107] R. Turrisi,[56] T. S. Tveter,[21] K. Ullaland,[22] E. N. Umaka,[125] A. Uras,[135] G. L. Usai,[24] A. Utrobicic,[97] M. Vala,[38,116] N. Valle,[139] S. Vallero,[58] N. van der Kolk,[63] L. V. R. van Doremalen,[63] M. van Leeuwen,[63] P. Vande Vyvre,[34] D. Varga,[145] Z. Varga,[145] M. Varga-Kofarago,[145] A. Vargas,[44] M. Vargyas,[126] R. Varma,[48] M. Vasileiou,[82] A. Vasiliev,[86] O. Vázquez Doce,[103,117] V. Vechernin,[112] A. M. Veen,[63] E. Vercellin,[26] S. Vergara Limón,[44] L. Vermunt,[63] R. Vernet,[7] R. Vértesi,[145] M. G. D. L. C. Vicencio,[9] L. Vickovic,[35] J. Viinikainen,[126] Z. Vilakazi,[131] O. Villalobos Baillie,[109] A. Villatoro Tello,[44] G. Vino,[52] A. Vinogradov,[86] T. Virgili,[30] V. Vislavicius,[87] A. Vodopyanov,[74] B. Volkel,[34] M. A. Völkl,[101] K. Voloshin,[90] S. A. Voloshin,[143] G. Volpe,[33] B. von Haller,[34] I. Vorobyev,[103] D. Voscek,[116] J. Vrláková,[38] B. Wagner,[22] M. Weber,[113] S. G. Weber,[105,144] A. Wegrzynek,[34] D. F. Weiser,[102] S. C. Wenzel,[34] J. P. Wessels,[144] E. Widmann,[113] J. Wiechula,[68] J. Wikne,[21] G. Wilk,[83] J. Wilkinson,[53] G. A. Willems,[34] E. Willsher,[109] B. Windelband,[102] W. E. Witt,[130] Y. Wu,[128] R. Xu,[6] S. Yalcin,[76] K. Yamakawa,[45] S. Yang,[22] S. Yano,[137] Z. Yin,[6] H. Yokoyama,[63,133] I.-K. Yoo,[18] J. H. Yoon,[60] S. Yuan,[22] A. Yuncu,[102] V. Yurchenko,[2] V. Zaccolo,[25,58] A. Zaman,[15] C. Zampolli,[34] H. J. C. Zanoli,[63,121] N. Zardoshti,[34] A. Zarochentsev,[112] P. Závada,[66] N. Zaviyalov,[107] H. Zbroszczyk,[142] M. Zhalov,[96] X. Zhang,[6] Z. Zhang,[6] C. Zhao,[21] V. Zherebchevskii,[112] N. Zhigareva,[90] D. Zhou,[6] Y. Zhou,[87] Z. Zhou,[22] J. Zhu,[6] Y. Zhu,[6] A. Zichichi,[10,27] M. B. Zimmermann,[34] G. Zinovjev,[2] and N. Zurlo[140]

(ALICE Collaboration)

[1]*A. I. Alikhanyan National Science Laboratory (Yerevan Physics Institute) Foundation, Yerevan, Armenia*
[2]*Bogolyubov Institute for Theoretical Physics, National Academy of Sciences of Ukraine, Kiev, Ukraine*
[3]*Bose Institute, Department of Physics and Centre for Astroparticle Physics and Space Science (CAPSS), Kolkata, India*
[4]*Budker Institute for Nuclear Physics, Novosibirsk, Russia*
[5]*California Polytechnic State University, San Luis Obispo, California, USA*
[6]*Central China Normal University, Wuhan, China*
[7]*Centre de Calcul de l'IN2P3, Villeurbanne, Lyon, France*
[8]*Centro de Aplicaciones Tecnológicas y Desarrollo Nuclear (CEADEN), Havana, Cuba*
[9]*Centro de Investigación y de Estudios Avanzados (CINVESTAV), Mexico City and Mérida, Mexico*
[10]*Centro Fermi - Museo Storico della Fisica e Centro Studi e Ricerche "Enrico Fermi," Rome, Italy*
[11]*Chicago State University, Chicago, Illinois, USA*
[12]*China Institute of Atomic Energy, Beijing, China*
[13]*Chonbuk National University, Jeonju, Republic of Korea*
[14]*Comenius University Bratislava, Faculty of Mathematics, Physics and Informatics, Bratislava, Slovakia*
[15]*COMSATS University Islamabad, Islamabad, Pakistan*
[16]*Creighton University, Omaha, Nebraska, USA*
[17]*Department of Physics, Aligarh Muslim University, Aligarh, India*
[18]*Department of Physics, Pusan National University, Pusan, Republic of Korea*
[19]*Department of Physics, Sejong University, Seoul, Republic of Korea*
[20]*Department of Physics, University of California, Berkeley, California, USA*
[21]*Department of Physics, University of Oslo, Oslo, Norway*
[22]*Department of Physics and Technology, University of Bergen, Bergen, Norway*
[23]*Dipartimento di Fisica dell'Università "La Sapienza" and Sezione INFN, Rome, Italy*
[24]*Dipartimento di Fisica dell'Università and Sezione INFN, Cagliari, Italy*
[25]*Dipartimento di Fisica dell'Università and Sezione INFN, Trieste, Italy*
[26]*Dipartimento di Fisica dell'Università and Sezione INFN, Turin, Italy*
[27]*Dipartimento di Fisica e Astronomia dell'Università and Sezione INFN, Bologna, Italy*
[28]*Dipartimento di Fisica e Astronomia dell'Università and Sezione INFN, Catania, Italy*
[29]*Dipartimento di Fisica e Astronomia dell'Università and Sezione INFN, Padova, Italy*
[30]*Dipartimento di Fisica "E.R. Caianiello" dell'Università and Gruppo Collegato INFN, Salerno, Italy*
[31]*Dipartimento DISAT del Politecnico and Sezione INFN, Turin, Italy*
[32]*Dipartimento di Scienze e Innovazione Tecnologica dell'Università del Piemonte Orientale and INFN Sezione di Torino, Alessandria, Italy*
[33]*Dipartimento Interateneo di Fisica "M. Merlin" and Sezione INFN, Bari, Italy*
[34]*European Organization for Nuclear Research (CERN), Geneva, Switzerland*
[35]*Faculty of Electrical Engineering, Mechanical Engineering and Naval Architecture, University of Split, Split, Croatia*
[36]*Faculty of Engineering and Science, Western Norway University of Applied Sciences, Bergen, Norway*
[37]*Faculty of Nuclear Sciences and Physical Engineering, Czech Technical University in Prague, Prague, Czech Republic*
[38]*Faculty of Science, P.J. Šafárik University, Košice, Slovakia*
[39]*Frankfurt Institute for Advanced Studies, Johann Wolfgang Goethe-Universität Frankfurt, Frankfurt, Germany*
[40]*Gangneung-Wonju National University, Gangneung, Republic of Korea*

[41]*Gauhati University, Department of Physics, Guwahati, India*
[42]*Helmholtz-Institut für Strahlen- und Kernphysik, Rheinische Friedrich-Wilhelms-Universität Bonn, Bonn, Germany*
[43]*Helsinki Institute of Physics (HIP), Helsinki, Finland*
[44]*High Energy Physics Group, Universidad Autónoma de Puebla, Puebla, Mexico*
[45]*Hiroshima University, Hiroshima, Japan*
[46]*Hochschule Worms, Zentrum für Technologietransfer und Telekommunikation (ZTT), Worms, Germany*
[47]*Horia Hulubei National Institute of Physics and Nuclear Engineering, Bucharest, Romania*
[48]*Indian Institute of Technology Bombay (IIT), Mumbai, India*
[49]*Indian Institute of Technology Indore, Indore, India*
[50]*Indonesian Institute of Sciences, Jakarta, Indonesia*
[51]*INFN, Laboratori Nazionali di Frascati, Frascati, Italy*
[52]*INFN, Sezione di Bari, Bari, Italy*
[53]*INFN, Sezione di Bologna, Bologna, Italy*
[54]*INFN, Sezione di Cagliari, Cagliari, Italy*
[55]*INFN, Sezione di Catania, Catania, Italy*
[56]*INFN, Sezione di Padova, Padova, Italy*
[57]*INFN, Sezione di Roma, Rome, Italy*
[58]*INFN, Sezione di Torino, Turin, Italy*
[59]*INFN, Sezione di Trieste, Trieste, Italy*
[60]*Inha University, Incheon, Republic of Korea*
[61]*Institut de Physique Nucléaire d'Orsay (IPNO), Institut National de Physique Nucléaire et de Physique des Particules (IN2P3/CNRS), Université de Paris-Sud, Université Paris-Saclay, Orsay, France*
[62]*Institute for Nuclear Research, Academy of Sciences, Moscow, Russia*
[63]*Institute for Subatomic Physics, Utrecht University/Nikhef, Utrecht, Netherlands*
[64]*Institute of Experimental Physics, Slovak Academy of Sciences, Košice, Slovakia*
[65]*Institute of Physics, Homi Bhabha National Institute, Bhubaneswar, India*
[66]*Institute of Physics of the Czech Academy of Sciences, Prague, Czech Republic*
[67]*Institute of Space Science (ISS), Bucharest, Romania*
[68]*Institut für Kernphysik, Johann Wolfgang Goethe-Universität Frankfurt, Frankfurt, Germany*
[69]*Instituto de Ciencias Nucleares, Universidad Nacional Autónoma de México, Mexico City, Mexico*
[70]*Instituto de Física, Universidade Federal do Rio Grande do Sul (UFRGS), Porto Alegre, Brazil*
[71]*Instituto de Física, Universidad Nacional Autónoma de México, Mexico City, Mexico*
[72]*iThemba LABS, National Research Foundation, Somerset West, South Africa*
[73]*Johann-Wolfgang-Goethe Universität Frankfurt Institut für Informatik, Fachbereich Informatik und Mathematik, Frankfurt, Germany*
[74]*Joint Institute for Nuclear Research (JINR), Dubna, Russia*
[75]*Korea Institute of Science and Technology Information, Daejeon, Republic of Korea*
[76]*KTO Karatay University, Konya, Turkey*
[77]*Laboratoire de Physique Subatomique et de Cosmologie, Université Grenoble-Alpes, CNRS-IN2P3, Grenoble, France*
[78]*Lawrence Berkeley National Laboratory, Berkeley, California, USA*
[79]*Lund University Department of Physics, Division of Particle Physics, Lund, Sweden*
[80]*Nagasaki Institute of Applied Science, Nagasaki, Japan*
[81]*Nara Women's University (NWU), Nara, Japan*
[82]*National and Kapodistrian University of Athens, School of Science, Department of Physics, Athens, Greece*
[83]*National Centre for Nuclear Research, Warsaw, Poland*
[84]*National Institute of Science Education and Research, Homi Bhabha National Institute, Jatni, India*
[85]*National Nuclear Research Center, Baku, Azerbaijan*
[86]*National Research Centre Kurchatov Institute, Moscow, Russia*
[87]*Niels Bohr Institute, University of Copenhagen, Copenhagen, Denmark*
[88]*Nikhef, National institute for subatomic physics, Amsterdam, Netherlands*
[89]*NRC Kurchatov Institute IHEP, Protvino, Russia*
[90]*NRC Kurchatov Institute - ITEP, Moscow, Russia*
[91]*NRNU Moscow Engineering Physics Institute, Moscow, Russia*
[92]*Nuclear Physics Group, STFC Daresbury Laboratory, Daresbury, United Kingdom*
[93]*Nuclear Physics Institute of the Czech Academy of Sciences, Řež u Prahy, Czech Republic*
[94]*Oak Ridge National Laboratory, Oak Ridge, Tennessee, USA*
[95]*Ohio State University, Columbus, Ohio, USA*
[96]*Petersburg Nuclear Physics Institute, Gatchina, Russia*
[97]*Physics department, Faculty of science, University of Zagreb, Zagreb, Croatia*
[98]*Physics Department, Panjab University, Chandigarh, India*

[99] *Physics Department, University of Jammu, Jammu, India*
[100] *Physics Department, University of Rajasthan, Jaipur, India*
[101] *Physikalisches Institut, Eberhard-Karls-Universität Tübingen, Tübingen, Germany*
[102] *Physikalisches Institut, Ruprecht-Karls-Universität Heidelberg, Heidelberg, Germany*
[103] *Physik Department, Technische Universität München, Munich, Germany*
[104] *Politecnico di Bari, Bari, Italy*
[105] *Research Division and ExtreMe Matter Institute EMMI, GSI Helmholtzzentrum für Schwerionenforschung GmbH, Darmstadt, Germany*
[106] *Rudjer Bošković Institute, Zagreb, Croatia*
[107] *Russian Federal Nuclear Center (VNIIEF), Sarov, Russia*
[108] *Saha Institute of Nuclear Physics, Homi Bhabha National Institute, Kolkata, India*
[109] *School of Physics and Astronomy, University of Birmingham, Birmingham, United Kingdom*
[110] *Sección Física, Departamento de Ciencias, Pontificia Universidad Católica del Perú, Lima, Peru*
[111] *Shanghai Institute of Applied Physics, Shanghai, China*
[112] *St. Petersburg State University, St. Petersburg, Russia*
[113] *Stefan Meyer Institut für Subatomare Physik (SMI), Vienna, Austria*
[114] *SUBATECH, IMT Atlantique, Université de Nantes, CNRS-IN2P3, Nantes, France*
[115] *Suranaree University of Technology, Nakhon Ratchasima, Thailand*
[116] *Technical University of Košice, Košice, Slovakia*
[117] *Technische Universität München, Excellence Cluster "Universe," Munich, Germany*
[118] *The Henryk Niewodniczanski Institute of Nuclear Physics, Polish Academy of Sciences, Cracow, Poland*
[119] *The University of Texas at Austin, Austin, Texas, USA*
[120] *Universidad Autónoma de Sinaloa, Culiacán, Mexico*
[121] *Universidade de São Paulo (USP), São Paulo, Brazil*
[122] *Universidade Estadual de Campinas (UNICAMP), Campinas, Brazil*
[123] *Universidade Federal do ABC, Santo Andre, Brazil*
[124] *University of Cape Town, Cape Town, South Africa*
[125] *University of Houston, Houston, Texas, USA*
[126] *University of Jyväskylä, Jyväskylä, Finland*
[127] *University of Liverpool, Liverpool, United Kingdom*
[128] *University of Science and Techonology of China, Hefei, China*
[129] *University of South-Eastern Norway, Tonsberg, Norway*
[130] *University of Tennessee, Knoxville, Tennessee, USA*
[131] *University of the Witwatersrand, Johannesburg, South Africa*
[132] *University of Tokyo, Tokyo, Japan*
[133] *University of Tsukuba, Tsukuba, Japan*
[134] *Université Clermont Auvergne, CNRS/IN2P3, LPC, Clermont-Ferrand, France*
[135] *Université de Lyon, Université Lyon 1, CNRS/IN2P3, IPN-Lyon, Villeurbanne, Lyon, France*
[136] *Université de Strasbourg, CNRS, IPHC UMR 7178, F-67000 Strasbourg, France, Strasbourg, France*
[137] *Université Paris-Saclay Centre d'Etudes de Saclay (CEA), IRFU, Départment de Physique Nucléaire (DPhN), Saclay, France*
[138] *Università degli Studi di Foggia, Foggia, Italy*
[139] *Università degli Studi di Pavia, Pavia, Italy*
[140] *Università di Brescia, Brescia, Italy*
[141] *Variable Energy Cyclotron Centre, Homi Bhabha National Institute, Kolkata, India*
[142] *Warsaw University of Technology, Warsaw, Poland*
[143] *Wayne State University, Detroit, Michigan, USA*
[144] *Westfälische Wilhelms-Universität Münster, Institut für Kernphysik, Münster, Germany*
[145] *Wigner Research Centre for Physics, Hungarian Academy of Sciences, Budapest, Hungary*
[146] *Yale University, New Haven, Connecticut, USA*
[147] *Yonsei University, Seoul, Republic of Korea*

[a]Present address: Dipartimento DET del Politecnico di Torino, Turin, Italy.
[b]Present address: M.V. Lomonosov Moscow State University, D.V. Skobeltsyn Institute of Nuclear, Physics, Moscow, Russia.
[c]Deceased.
[d]Present address: Department of Applied Physics, Aligarh Muslim University, Aligarh, India.
[e]Present address: Institute of Theoretical Physics, University of Wroclaw, Poland.